

SoK: Security Evaluation of Wi-Fi CSI Biometrics: Attacks, Metrics, and Systemic Weaknesses

Giuliano de Oliveira Braga, Pedro Henrique dos Santos Rocha, Rafael Pimenta de Mattos Paixão, Giovanni Hoff da Costa, Gustavo Cavalcanti Morais, Lourenço Alves Pereira Júnior

Aeronautics Institute of Technology (ITA)

São José dos Campos, SP, Brazil

{giulianobraga,psrocha,paixao,giovani.costa.60940,gustavomorais,ljr}@ita.br

Abstract—Wi-Fi Channel State Information (CSI) has been repeatedly proposed as a biometric modality, often with reports of high accuracy and operational feasibility. However, the field lacks a consolidated understanding of its security properties, adversarial resilience, and methodological consistency. This Systematization of Knowledge (SoK) examines CSI-based biometric authentication through a security perspective, analyzing how existing work differs across sensing infrastructure, signal representations, feature pipelines, learning models, and evaluation methodologies. Our synthesis reveals systemic inconsistencies: reliance on aggregate accuracy metrics, limited reporting of FAR/FRR/EER, absence of per-user risk analysis, and scarce consideration of threat models or adversarial feasibility. We construct a unified evaluation framework to empirically expose these issues and demonstrate how security-relevant metrics, such as per-class EER, FCS, and the Gini Coefficient, uncover risk concentration that remains hidden under traditional reporting practices. Our analysis highlights concrete attack surfaces and shows how methodological choices materially influence vulnerability profiles, which include replay, geometric mimicry, and environmental perturbation. Based on these findings, we articulate the security boundaries of current CSI biometrics and provide guidelines for rigorous evaluation, reproducible experimentation, and future research directions. This SoK offers the security community a structured, evidence-driven reassessment of Wi-Fi CSI biometrics and their suitability as an authentication primitive.

Index Terms—Wi-Fi CSI, Authentication, Biometrics, Feature Importance, Metrics.

I. INTRODUCTION

User authentication remains one of the core challenges in modern cybersecurity [1]. Physical-layer biometrics, which rely on intrinsic physiological and behavioral traits, offer a compelling alternative by removing the need for explicit user actions or dedicated sensing hardware.

Wi-Fi Channel State Information (CSI) has gained prominence as a versatile sensing modality for human-centric applications, capturing subtle variations in wireless propagation caused by a person’s presence, movements, and intrinsic attributes [2], [3]. In contrast to conventional RSSI, CSI exposes amplitude and phase measurements at the subcarrier level, providing much finer spatial and temporal resolution. Its complex-valued structure encodes distinctive electromagnetic patterns shaped by an individual’s body geometry, tissue properties, and attitude patterns.

The literature on CSI-based biometric authentication has evolved along multiple dimensions. Dynamic authentication systems exploit temporal behavioral patterns such as gait [4], [5], keystroke dynamics [6], and gestures [7]. These approaches leverage spatiotemporal CSI variations to capture unique user behaviors, demonstrating high accuracy [6]. However, dynamic systems inherently face challenges related to motion artifacts and the need for consistent behavioral patterns. In contrast, static authentication systems focus on geometric and radiometric properties captured through stable electromagnetic interactions, such as palm placement [1], [2], [8]. These approaches help reduce motion artifacts and yield more repeatable measurements, making them suitable for scenarios that require consistent positioning—identifying a person by who they are rather than by what they know or do. Behavioral authentication systems extend this by exploiting walking and stationary patterns during daily activities for continuous authentication, though they face challenges from environmental interference and multiple individuals [9]. Multi-frequency approaches have been explored to enhance robustness and discriminative power by combining information from multiple frequency bands [10], albeit requiring more complex hardware and increased computational complexity. Advanced applications of CSI sensing also extend beyond authentication to include 3D human pose estimation [11], [12] and secret key generation [13]. These advanced approaches, however, rely on sophisticated deep learning architectures and substantial computational resources.

Unfortunately, despite substantial progress in CSI-based research, several critical challenges persist in the broader field of physiological biometric authentication. The area still suffers from a limited number of studies, fragmented methodologies, and inconsistent validation practices, making it difficult to assess whether reported improvements reflect real and meaningful advances. Reproducibility issues are common, often stemming from dependence on proprietary hardware (e.g., the Intel 5300 NIC) or insufficient implementation details. Moreover, many studies report only basic accuracy metrics while overlooking essential security-oriented measures such as Equal Error Rate (EER), False Acceptance Rate (FAR), and False Rejection Rate (FRR). These omissions frequently occur alongside a lack of auxiliary statistical analyses—such as score-distribution modeling or subject-level fairness evalu-

ation—which are crucial for ensuring robustness in real-world deployments.

This Systematization of Knowledge (SoK) addresses these gaps by introducing a unified framework for Wi-Fi CSI-based static physiological biometric authentication, emphasizing reproducibility and standardization. We integrate fragmented methodologies into a single pipeline that spans raw CSI acquisition through machine-learning inference. Our approach combines physics-based principles—rooted in Maxwell’s equations and their impact on amplitude, phase, and energy profiles—with data-driven techniques such as statistical filtering, normalization, and security-focused evaluation metrics.

A. Motivation

The motivation for Wi-Fi CSI-based static physiological biometric authentication lies in its clear advantages as an additional security factor. It operates non-intrusively, requiring no user interaction or wearable sensors, and leverages existing Wi-Fi infrastructure—avoiding the existing vulnerabilities and costs of specialized hardware [14].

CSI is also highly cost-effective: it can be extracted from commodity Wi-Fi devices using open-source tools like Nexmon [15] and deployed on low-cost platforms such as the Raspberry Pi, making it suitable for large-scale and resource-constrained environments.

Moreover, CSI-based sensing adds a complementary security layer to systems that rely on dedicated devices or ID cards. This is especially valuable in access control and continuous authentication scenarios where explicit user interaction can be impractical.

Additionally, the growing ubiquity of Wi-Fi networks—along with the standardization of IEEE 802.11bf—further strengthens this approach. As Wi-Fi infrastructure becomes pervasive, CSI-based systems can operate on existing deployments without additional hardware, enabling scalable and practical real-world adoption.

B. Scope and Objective

To provide a reproducible framework for static physiological biometric authentication, this work focuses on the physical-layer representation of the wireless channel as a means of identifying individuals through their electromagnetic interaction with the propagation field. Our study targets **static palm-based identification for robust authentication**, with the subject’s hand positioned approximately 5 cm above the Raspberry Pi 4B antenna—capturing fine radiometric and geometric patterns while minimizing motion artifacts and ensuring repeatable measurements.

The experiment used the 5 GHz Wi-Fi band, where the increased granularity and field perturbations enhance the discriminative power of CSI amplitude and phase features [16]. In addition, this band exhibits lower amplitude variability—and thus reduced noise—compared to 2.4 GHz [17], while offering superior stability and better temporal resolution under a 40 MHz bandwidth than under 20 MHz [18], [19]. Together, these factors contribute to improved model performance [20].

Another characteristic of lower frequencies in Wi-Fi systems is their relationship with Free-Space Path Loss (FSPL). Although these frequencies offer extended range, they also exhibit increased susceptibility to environmental interference due to the proliferation of consumer electronic devices in daily use [3], [18].

The primary objective is to unify the fragmented methodologies across the literature into a coherent pipeline that spans from raw CSI acquisition to feature extraction and machine learning classification. In this way, the approach thus bridges the gap between theoretical electromagnetics and practical biometric intelligence.

Within this scope, the study aims to establish a consistent experimental foundation using commodity Wi-Fi hardware and open-source tools (notably Nexmon). Furthermore, it seeks to define a unified preprocessing and feature-extraction methodology that preserves physical interpretability. The research then assesses multiple classifiers under controlled conditions to measure their discriminative power and robustness.

By framing CSI as both a physical quantity and a biometric signal “meter”, this work advances the systematization of CSI-based static authentication research, providing a transparent, replicable, and physics-aware benchmark for future studies.

C. Contributions

- Taxonomy of CSI-based biometric systems.
- Experimental validation with static-hand dataset.
- Unified feature extraction and classification pipeline.
- Discussion on reproducibility and metrics for biometric authentication systems.

The remainder of this paper is organized as follows: Section II provides background on Wi-Fi CSI and the theoretical basis for feature extraction. Section III systematizes prior work via a structured taxonomy and comprehensive benchmark comparison. Section IV details the unified reproducible pipeline. Section V presents experimental validation results demonstrating the feasibility of static palm-based authentication. Section VI discusses strengths, limitations, and security implications. Section VII explores future research directions, including anomaly detection and the implications of IEEE 802.11bf standardization for Wi-Fi Sensing (WFS). Finally, Section VIII summarizes contributions, positioning this SoK as a foundational reference for advancing the field toward practical, deployable CSI-based biometric systems.

II. BACKGROUND ON WI-FI CSI AND BIOMETRIC SENSING

In real-world environments, wireless signals propagate along multiple paths due to reflections and refractions. Consequently, the received signal constitutes the superposition of these multipath components. The received signal spectrum, $R(k)$, is then formally related to the transmitted spectrum, $S(f)$, through the following frequency domain relationship [2], [21], [22]:

$$R(f) = S(f)H(f) + N(f) \quad (1)$$

where $H(f)$ represents the CSI. Equation (1) serves as the foundation for the extraction of complex CSI data from the Raspberry Pi 4B using the Nexmon tool, a process which will be detailed in Section II-K.

The channel frequency response (CFR), denoted as $H(f)$, constitutes the complex transfer function of the wireless channel [3], [21], [23]:

$$H(f) = |H(f)|e^{j\phi(f)} \quad (2)$$

where $|H(k)|$ is the magnitude response and $\phi(k)$ is the phase response. The Channel Impulse Response (CIR), $h(t)$, simultaneously represents the time-domain equivalent of the CSI [24]–[26]:

$$h(t) = \sum_{n=1}^N \alpha_n e^{-j\phi_n} \delta(t - \tau_n) \quad (3)$$

where α_n , ϕ_n , and τ_n are the complex attenuation, phase, and time delay of the n^{th} path.

The following subsections detail the features extracted from the complex CSI data. These features were derived from related works and specific experimentations carried out in this study. This approach was adopted because some of these features, despite not being directly related to the premise of our study (static authentication), demonstrated subtle performance improvements when included in the model training.

A. Magnitude-Based Features: Ampère-Maxwell Law

In the experimental context, the measured amplitude variations across subcarriers represent fluctuations in the electromagnetic energy induced by each subject's presence and body geometry [11]. Thus, analyzing these magnitude-based features enables quantifying the dynamic redistribution of current density and field intensity in the Wi-Fi propagation path, serving as a physical proxy for identifying individual radiometric signatures [27].

B. Fundamental Magnitude Calculation

The amplitude response of the channel that can be extracted from complex CSI data is represented by [8], [28], [29]:

$$|H(f)| = \sqrt{\text{Re}^2\{H(f)\} + \text{Im}^2\{H(f)\}} \quad (4)$$

This magnitude calculation serves as the foundation for deriving the remaining amplitude features.

1) *Amplitude Mean Features*: The mean amplitude value across subcarriers and sample blocks is computed using the expression (5). Similarly, the standard deviation of the amplitude across these subcarriers and sample blocks is given by an similar formula (6). Analogous to this mean calculation, the standard deviation of the amplitude variance across subcarriers is determined by the expression presented in Equation (7). Furthermore, the statistical variance of the amplitude over the sampling period is independently determined by the mathematical representation in (8). [30]–[33]:

$$\text{amp_mean} = \frac{1}{K} \sum_{k=1}^K \frac{1}{T} \sum_{t=1}^T |H(f_k, t)| \quad (5)$$

where K and T are the number of subcarriers and time samples, respectively.

$\text{amp_mean_std} =$

$$\sqrt{\frac{1}{K-1} \sum_{k=1}^K \left(\frac{1}{T} \sum_{t=1}^T |H(f_k, t)| - \text{amp_mean} \right)^2} \quad (6)$$

$\text{amp_var_mean} =$

$$\frac{1}{K} \sum_{k=1}^K \frac{1}{T-1} \sum_{t=1}^T \left(|H(f_k, t)| - \frac{1}{T} \sum_{t'=1}^T |H(f_k, t')| \right)^2 \quad (7)$$

$\text{amp_var_std} =$

$$\sqrt{\frac{1}{K-1} \sum_{k=1}^K (\text{Var}_k\{|H(f_k, t)|\} - \text{amp_var_mean})^2} \quad (8)$$

Other key features arising from the CSI amplitude include skewness (9) and kurtosis (10), which serve to characterize the palm's reflection pattern, as they enable the identification of specific peaks and tails unique to each user.

2) *Amplitude Statistical Moments*: The hand of each subject induces distinct attenuations and resonances in the subcarriers, a phenomenon contingent upon physiological factors such as tissue thickness, bone and tendon structure, skin moisture, geometry, and others. Consequently, the spectral asymmetry tends to exhibit a consistent pattern across individuals, thereby acting as a unique frequency signature (such as "palmprint") [5], [34], [35].

The skewness of the amplitude distribution across the subcarriers is defined as:

$$\text{amp_skew_mean} = \frac{1}{K} \sum_{k=1}^K \frac{\mathbb{E} \left[(|H(f_k, t)| - \mu_k)^3 \right]}{\sigma_k^3} \quad (9)$$

Conversely, the distribution of the fourth moment of amplitude (amplitude kurtosis) across subcarriers is determined by:

$$\text{amp_kurt_mean} = \frac{1}{K} \sum_{k=1}^K \frac{\mathbb{E} \left[(|H(f_k, t)| - \mu_k)^4 \right]}{\sigma_k^4} - 3 \quad (10)$$

C. Phase-Based Features: Faraday Law

Equivalent to the analysis performed on the CSI amplitude, the phase components were subjected to the same extraction process. Our work applied the heuristics established in Section IV to derive features from the phase data.

1) *Fundamental Phase Calculation*: The phase of the CSI formally defines the phase response of the wireless channel [29]:

$$\phi(f) = \arctan \left(\frac{\text{Im}\{H(f)\}}{\text{Re}\{H(f)\}} \right) \quad (11)$$

2) *Phase Mean Features*: The mean phase across subcarriers is computed to enhance robustness, and is given by the following expression:

$$\text{phase_mean_mean} = \frac{1}{K} \sum_{k=1}^K \frac{1}{T} \sum_{t=1}^T \phi(f_k, t) \quad (12)$$

The mean and standard deviation of the phase standard deviations across subcarriers are determined by the following formulas [36]–[38]:

$\text{phase_std_mean} =$

$$\frac{1}{K} \sum_{k=1}^K \sqrt{\frac{1}{T-1} \sum_{t=1}^T \left(\phi(f_k, t) - \frac{1}{T} \sum_{t'=1}^T \phi(f_k, t') \right)^2} \quad (13)$$

$\text{phase_std_std} =$

$$\sqrt{\frac{1}{K-1} \sum_{k=1}^K (\text{Std}_k\{\phi(f_k, t)\} - \text{phase_std_mean})^2} \quad (14)$$

3) *Phase Texture Features*: These features leverage the phase gradient (15) between adjacent subcarriers to mitigate hardware-induced errors (Carrier Frequency Offset - CFO/Sampling Frequency Offset - SFO) [39]. The dispersion analysis (expressions 16 and 17) quantifies the unique phase texture generated by both the user's geometry and behavior. This capability allows for the extraction of reliable temporal change patterns, even in dynamic environments, which is fundamental for fine-grained authentication [40]–[42]. Furthermore, the CSI phase usually unexplored due to its inherent susceptibility to timing errors. Consequently, investigating a robust phase processing methodology capable of extracting stable environmental information is paramount for achieving enhanced classification performance [43].

The phase gradient, or the difference between adjacent phases, is determined by the following equation:

$$\Delta\phi(f_k, t) = \phi(f_{k+1}, t) - \phi(f_k, t) \quad (15)$$

The mean and standard deviation of the phase difference standard deviations are expressed by the following formulas:

$\text{dphi_std_mean} =$

$$\frac{1}{K-1} \sum_{k=1}^{K-1} \sqrt{\frac{1}{T-1} \sum_{t=1}^T \left(\Delta\phi(f_k, t) - \frac{1}{T} \sum_{t'=1}^T \Delta\phi(f_k, t') \right)^2} \quad (16)$$

$\text{dphi_std_std} =$

$$\sqrt{\frac{1}{K-2} \sum_{k=1}^{K-1} (\text{Std}_t\{\Delta\phi(f_k, t)\} - \text{dphi_std_mean})^2} \quad (17)$$

D. Energy-Based Features: Poynting Theorem

This topic outlines the methodology for extracting features based on the average power reflected and absorbed by the subcarriers. These features are designed to capture distinct scattering patterns among individuals, as well as to differentiate users based on reflection selectivity [44], [45].

Furthermore, they quantify the degree of scattering induced by each user's hand.

1) *Fundamental Energy Calculation*: The fundamental energy per subcarrier is derived from the square of the magnitude. [46], [47]:

$$E(f_k) = \frac{1}{T} \sum_{t=1}^T |H(f_k, t)|^2 \quad (18)$$

$E(f_k)$ provides a computationally tractable method for estimating the energy propagated, reflected, and absorbed by the human body, circumventing the need for direct field measurements by merely observing the CSI.

2) *Energy Distribution Features*: The Skewness and Kurtosis metrics are instrumental in deriving unique energy characteristics from the observed CSI. They quantify the body's contour and the magnitude of the user's motion. Analysis of the energy distribution across subcarriers then enables high-granularity user differentiation [4], [48]:

$$\text{energy_skewness} = \frac{\mathbb{E} \left[(E(f_k) - \mu_E)^3 \right]}{\sigma_E^3} \quad (19)$$

$$\text{energy_kurtosis} = \frac{\mathbb{E} \left[(E(f_k) - \mu_E)^4 \right]}{\sigma_E^4} - 3 \quad (20)$$

Entropy quantifies the uniformity of energy distribution across subcarriers, thereby generating a robust feature suitable for profile uniqueness in authentication [16], [49]:

$$\text{energy_entropy} = - \sum_{k=1}^K p(f_k) \log_2 p(f_k) \quad (21)$$

where $p(f_k) = \frac{E(f_k)}{\sum_{k'=1}^K E(f_{k'})}$ is the normalized energy distribution.

E. Spectral Analysis Features: Wave Equation

The spectral features (22-26) are utilized to quantify the distribution of CSI energy per subcarrier. They are vital for capturing fine patterns (e.g., biometrics or gestures), differentiating spectral noise (24), and enabling robust authentication and high-granularity recognition within the Wi-Fi CSI systems [50]–[54].

1) *Spectral Centroid*: The spectral centroid represents the center of mass of the magnitude spectrum:

$$\text{spec_centroid} = \frac{\sum_{k=1}^K f_k \cdot |H(f_k)|}{\sum_{k=1}^K |H(f_k)|} \quad (22)$$

2) *Spectral Entropy*: The spectral entropy measures the uniformity of the magnitude spectrum:

$\text{spec_entropy} =$

$$- \sum_{k=1}^K \frac{|H(f_k)|}{\sum_{k'=1}^K |H(f_{k'})|} \log_2 \left(\frac{|H(f_k)|}{\sum_{k'=1}^K |H(f_{k'})|} \right) \quad (23)$$

3) *Spectral Flatness*: The spectral flatness measures the noisiness of the spectrum:

$$\text{spec_flatness} = \frac{\sqrt[\kappa]{\prod_{k=1}^K |H(f_k)|}}{\frac{1}{K} \sum_{k=1}^K |H(f_k)|} \quad (24)$$

4) *Advanced Spectral Features*: The spectral centroid for amplitude analysis:

$$\text{spectral_centroid_amp} = \frac{\sum_{k=1}^K k \cdot |H(f_k)|}{\sum_{k=1}^K |H(f_k)|} \quad (25)$$

The spectral width (second moment):

$$\text{spectral_width} = \sqrt{\frac{\sum_{k=1}^K (k - \text{spectral_centroid_amp})^2 \cdot |H(f_k)|}{\sum_{k=1}^K |H(f_k)|}} \quad (26)$$

F. Empirical Energy Features: Energy Conservation

1) *Empirical Energy Model*: The features, in this section, decompose the CSI energy into its fundamental components: Reflection (27), Absorption (28) (attributable to biophysical factors), and Refraction (29) (linked to motion or phase shifts). The result of this decomposition is the formation of a “unique physical signature”, which is paramount for achieving robust authentication and fine-grained recognition [27], [55]–[58]. Specifically, this approach quantifies the subject’s physical interaction with the Wi-Fi signal, thus rendering the signature highly resistant to forgery [1].

2) *Reflected Energy*: Energy above the mean represents reflected components:

$$R_{\text{emp}} = \frac{\mathbb{E}[E(f_k) | E(f_k) \geq \mu_E]}{\mu_E} \quad (27)$$

where $\mu_E = \frac{1}{K} \sum_{k=1}^K E(f_k)$ is the mean energy.

3) *Absorbed Energy*: Energy below the mean represents absorbed components:

$$A_{\text{emp}} = \frac{\mathbb{E}[E(f_k) | E(f_k) < \mu_E]}{\mu_E} \quad (28)$$

4) *Refracted Energy*: Phase variation represents refracted/dispersed energy:

$$T_{\text{emp}} = \frac{\mathbb{E}[\sigma_\phi(f_k)]}{\pi} \quad (29)$$

where $\sigma_\phi(f_k)$ is the standard deviation of phase across time for subcarrier k .

5) *Normalized Empirical Energies*: The normalized empirical energy features used are:

$$\text{energy_reflected_emp} = \frac{R_{\text{emp}}}{R_{\text{emp}} + A_{\text{emp}} + T_{\text{emp}}} \quad (30)$$

$$\text{energy_absorbed_emp} = \frac{A_{\text{emp}}}{R_{\text{emp}} + A_{\text{emp}} + T_{\text{emp}}} \quad (31)$$

$$\text{energy_refracted_emp} = \frac{T_{\text{emp}}}{R_{\text{emp}} + A_{\text{emp}} + T_{\text{emp}}} \quad (32)$$

G. Temporal Variability Features

Temporal Variability (33-35) and Stability (36-38) features quantify the fluctuations in CSI amplitude across the time domain. This analysis is vital because distinct individuals induce unique variations in the CSI due to their inherent physiological and behavioral traits. These features (e.g., standard deviation) quantify the movement range and characterize identity uniqueness, making them essential for activity segmentation (via variance analysis) and for building robust user profiles necessary for fine-grained authentication [59]–[61]. Although our work does not handle movements, these features proved relevant for distinguishing subtle nuances among users, thereby yielding significant performance gains in metrics (e.g., precision, recall, and specificity) across the selected models.

1) *Temporal Variability Analysis*: The temporal variability measures fluctuations in magnitude over time:

$$\text{temporal_variability_mean} = \frac{1}{K} \sum_{k=1}^K \sqrt{\frac{1}{T-1} \sum_{t=1}^T \left(|H(f_k, t)| - \frac{1}{T} \sum_{t'=1}^T |H(f_k, t')| \right)^2} \quad (33)$$

The standard deviation of temporal variability:

$$\text{temporal_variability_std} = \sqrt{\frac{1}{K-1} \sum_{k=1}^K (\text{Std}_t\{|H(f_k, t)|\} - \text{temporal_variability_mean})^2} \quad (34)$$

The coefficient of variation:

$$\text{temporal_variability_cv} = \frac{\text{temporal_variability_mean}}{\frac{1}{K} \sum_{k=1}^K \frac{1}{T} \sum_{t=1}^T |H(f_k, t)|} \quad (35)$$

H. Stability Features

Stability features quantify the temporal consistency of CSI amplitude across subcarriers, measuring how uniformly each frequency bin maintains its magnitude over time. These metrics capture user-specific stability patterns through the coefficient of variation, enabling discrimination between individuals based on their unique temporal coherence signatures in the electromagnetic field.

1) *Stability Analysis*: The coefficient of variation for stability measurement:

$$\text{CV}_k = \frac{\text{Std}_t\{|H(f_k, t)|\}}{\mathbb{E}_t[|H(f_k, t)|]} \quad (36)$$

The mean coefficient of variation:

$$\text{stability_mean_cv} = \frac{1}{K} \sum_{k=1}^K \text{CV}_k \quad (37)$$

The standard deviation of coefficient of variation:

$$\text{stability_std_cv} = \sqrt{\frac{1}{K-1} \sum_{k=1}^K (\text{CV}_k - \text{stability_mean_cv})^2} \quad (38)$$

I. Spatial Correlation Features

The correlation between adjacent subcarriers serves to assess the spectral coherence of the CSI. This metric is also considered vital for authentication applications, as it facilitates the filtering of noisy or unstable subcarriers. Consequently, this ensures that the extracted features accurately represent the subject's unique physical interaction (radiobiometrics) with the Wi-Fi signal, thereby bolstering the system's resistance to fraudulent attempts [4], [62]–[64].

1) *Adjacent Subcarrier Correlation*: The correlation between adjacent subcarriers:

$$\rho_k = \frac{\text{Cov}(|H(f_k, t)|, |H(f_{k+1}, t)|)}{\sqrt{\text{Var}(|H(f_k, t)|)\text{Var}(|H(f_{k+1}, t)|)}} \quad (39)$$

The mean adjacent correlation:

$$\text{adjacent_correlation_mean} = \frac{1}{K-1} \sum_{k=1}^{K-1} \rho_k \quad (40)$$

The standard deviation of adjacent correlations:

adjacent_correlation_std =

$$\sqrt{\frac{1}{K-2} \sum_{k=1}^{K-1} (\rho_k - \text{adjacent_correlation_mean})^2} \quad (41)$$

2) *Spectral Roughness Analysis*: Spectral roughness quantifies the fine-grained irregularities in the amplitude response of the CSI spectrum across adjacent subcarriers. This metric captures local fluctuations that arise due to complex multipath interactions, constructive and destructive interference, and micro-differences in body morphology unique to each individual [53], [65].

The first-order spectral difference, or roughness, is computed as:

$$\Delta|H(f_k)| = |H(f_{k+1})| - |H(f_k)| \quad (42)$$

From this sequence, the mean and standard deviation of spectral roughness are derived as:

$$\text{spectral_roughness_mean} = \frac{1}{K-1} \sum_{k=1}^{K-1} |\Delta|H(f_k)|| \quad (43)$$

spectral_roughness_std =

$$\sqrt{\frac{1}{K-2} \sum_{k=1}^{K-1} (|\Delta|H(f_k)|| - \text{spectral_roughness_mean})^2} \quad (44)$$

A high *spectral_roughness_std* (44) value implies that the spectrum exhibits irregular amplitude transitions between subcarriers, while a lower value suggests a smoother, more uniform profile. This provides a quantitative indicator of individual-specific scattering diversity, often stable across captures of the same user but distinctive between different users [66].

3) *Spectral Curvature*: While roughness captures local amplitude differences, spectral curvature quantifies the rate of change of these variations—essentially describing the “bending” or morphological curvature of the CSI spectrum. This second-order derivative feature characterizes how energy rises and falls across frequency bins, encoding the smoothness or sharpness of the spectral envelope [67].

The curvature is computed as the second-order finite difference:

$$\Delta^2|H(f_k)| = |H(f_{k+2})| - 2|H(f_{k+1})| + |H(f_k)| \quad (45)$$

From this, the mean and standard deviation of spectral curvature are obtained as:

$$\text{spectral_curvature_mean} = \frac{1}{K-2} \sum_{k=1}^{K-2} |\Delta^2|H(f_k)|| \quad (46)$$

spectral_curvature_std =

$$\sqrt{\frac{1}{K-3} \sum_{k=1}^{K-2} (|\Delta^2|H(f_k)|| - \text{spectral_curvature_mean})^2} \quad (47)$$

Spectral curvature complements roughness by emphasizing higher-order spectral structures. Users with distinct body shapes, tissue dielectric constants, or positioning relative to the transceiver tend to induce unique curvature patterns, acting as high-resolution biometrics within the frequency domain [57]. When combined, the roughness–curvature pair provides a powerful representation of individual-specific propagation signatures.

J. Phase Calibration Formulas

Phase calibration formulas provide a systematic methodology to eliminate these hardware artifacts through sequential processing stages—offset removal, unwrapping, detrending, and normalization—thereby restoring the intrinsic phase response that encodes user-specific geometric and dielectric interactions with the wireless field [3], [33], [68].

1) *Non-linear Phase Calibration*: Following the methodology outlined in the Tsinghua University CSI tutorial [26], non-linear phase calibration is a multi-stage process designed to compensate for hardware-induced distortions. The raw CSI phase is often contaminated by hardware-induced errors, and Packet Detection Delay (PDD). These distortions introduce unpredictable phase drifts and linear biases that obscure the genuine propagation characteristics of the wireless channel.

2) *CFO Removal*: Carrier Frequency Offset originates from minor differences between the transmitter and receiver oscillators, leading to a constant phase shift across all subcarriers. To mitigate this, a global phase offset is subtracted from the CSI:

$$H_{\text{calib}}(f) = H(f) \cdot e^{-j\phi_{\text{offset}}} \quad (48)$$

where $\phi_{\text{offset}} = \text{median}(\phi(f))$ represents the median phase bias across subcarriers. This operation realigns the spectral phase reference, ensuring all subsequent processing reflects only propagation-related phase components rather than hardware drift.

3) *Phase Unwrapping*: Due to the periodic nature of the complex exponential representation, raw CSI phase values are confined to the interval $[-\pi, \pi]$. Consequently, abrupt 2π discontinuities appear between adjacent subcarriers or time samples. Phase unwrapping eliminates these discontinuities, reconstructing a continuous phase trajectory:

$$\phi_{\text{unwrapped}}(f_k) = \text{unwrap}(\phi(f_k)) \quad (49)$$

This step is essential for preserving genuine physical variations, such as those caused by path-length differences or small-scale user movements, which would otherwise appear as artificial phase jumps.

4) *Detrending*: After unwrapping, the CSI phase typically exhibits a linear bias induced by SFO and PDD. These effects introduce a linearly increasing phase trend across subcarriers. To compensate, a linear regression model is fitted and removed:

$$\phi_{\text{detrended}}(f_k) = \phi_{\text{unwrapped}}(f_k) - \text{linear_trend}(f_k) \quad (50)$$

Detrending isolates the residual phase fluctuations—those directly associated with the physical propagation environment—allowing subsequent analysis to focus on geometry-dependent variations attributable to user-specific scattering.

5) *Normalization*: Finally, the detrended phase is mean-centered to remove any remaining global bias:

$$\phi_{\text{normalized}}(f_k) = \phi_{\text{detrended}}(f_k) - \mathbb{E}[\phi_{\text{detrended}}(f_k)] \quad (51)$$

This normalization yields a zero-mean phase distribution, emphasizing relative rather than absolute phase characteristics. The resulting $\phi_{\text{normalized}}(f_k)$ captures the micro-variations of the wireless field induced by the subject’s geometry and posture, which are key discriminative signatures in CSI-based biometric systems [5], [27], [69].

K. CSI Acquisition Toolchain & Experimentation Setup

The CSI acquisition was performed using a customized open-source toolchain. Unlike legacy platforms such as Intel 5300 NIC [9], [70], [71], and Atheros CSI tools [72], which rely on desktop hardware, this study used the Nexmon framework [8], [16], [73] to extract CSI on embedded systems of IoT, enabling a fully portable, low-cost sensing platform based on the **Raspberry Pi 4B**.

1) *Hardware Components*: The experimental setup consisted of three principal devices:

- **Access Point (Receiver)**: TP-Link Archer C60 configured as the Wi-Fi access point (AP), operating under IEEE 802.11n mode on **Channel 36** (5180 MHz) with a **40 MHz** bandwidth under **IEEE 802.11n** modulation.
- **CSI Receiver (Sniffer)**: Raspberry Pi 4 Model B equipped with the BCM43455c0 wireless chipset, configured in **monitor mode** via Nexmon CSI. The receiver captured the raw Channel State Information (CSI) corresponding to 128 OFDM subcarriers over the 5180 MHz band, with a sampling configuration of **802.11n, Channel 36, 128-OFDM**.
- **Client (Transmitter)**: Samsung Galaxy Tab S9 FE (**64-QAM**) tablet running **iPerf2 for Android**, responsible for generating UDP traffic toward the TP-Link router to stimulate CSI variations in the wireless channel.

For experiment conducted, the Raspberry Pi was powered through a energy source with a USB output of **5 V/3.0 A**.

2) *Software and Configuration*: The CSI receiver was configured using the **Nexmon CSI** toolchain available in the official repository [15], [74], following the branch instructions for the Raspberry Pi kernel version 5.10.92. Nexmon provides firmware-level hooks that extract the raw CSI matrix ($H(f, t)$), preserving complex-valued amplitude and phase information per OFDM subcarrier.

The iPerf2 client was configured to transmit a continuous UDP flow toward the TP-Link router using the following parameters:

$$\text{iperf} -c 192.168.1.1 -u -b 500M -t 60 -i 1 -l 1400 -p 5500 \quad (52)$$

This command generates UDP packets (-u) to AP (-c) at a rate of 500 Mbits/s (-b) for 60 seconds (-t), using 1400-byte datagrams (-l) transmitted through port 5500 (-p), with reports generated every second (-i), ensuring the channel remains saturated and provides sufficient packet diversity for CSI sampling. Each subject underwent a total data acquisition period of two minutes. The protocol stipulated that the first minute involved five sample acquisitions from the left hand, and the subsequent minute involved five sample acquisitions from the right hand.

3) *Operational Overview*: During each session, the tablet sent UDP packets to the TP-Link router, while the Raspberry Pi—connected via Ethernet—passively captured CSI from incoming Wi-Fi frames, ensuring measurements reflected only the physical layer of the transmitter–router link.

The Raspberry Pi was connected via Ethernet to the router to facilitate the secure transfer of CSI data via SSH to the MSI GS63 Stealth 8RE laptop [75] immediately following each capture. The laptop was concurrently connected wirelessly to the TP-Link router, to storage repository for the acquired measurements.

The CSI data were stored in .pcap format and parsed via Nexmon’s Python interface into complex matrices $H(f_k, t) = a_{k,t} + jb_{k,t}$, where $a_{k,t}$ and $b_{k,t}$ are the real and imaginary components. Each .csv contained 128 subcarriers and variable rows per subject, capturing the CSI’s temporal evolution.

This toolchain thus combines low-cost hardware, open-source firmware, and standardized network utilities into a reproducible CSI measurement platform suitable for biometric experiments.

During all acquisition sessions, the participant’s right hand was positioned approximately **5 cm above the Raspberry Pi 4B’s antenna module**, ensuring a controlled static interaction zone for the captured CSI measurements.

III. SYSTEMATIZATION OF PRIOR WORK

This section organizes existing research on CSI-based biometrics through a structured taxonomy and compares representative works under a unified classification. We systematically review the state-of-the-art approaches, identifying their methodological patterns, evaluation protocols, and technological foundations to establish a comprehensive understanding of the field’s evolution and current state.

A. Taxonomy of CSI-Based Biometrics

To systematically compare CSI-based biometric systems, we propose a taxonomy based on five core dimensions: sensing infrastructure, signal domain, feature engineering, learning model, and evaluation protocol. Our experimental setup—Raspberry Pi 4B at 5 GHz, with a **focus on static gathering**, with or without mRMR-based feature selection, and MLP classification with 50-sample windows—fits into the category of device-based closed-set authentication using handcrafted features.

1) *Scope and Domain*: The scope of CSI-based biometric research spans multiple application domains, ranging from user authentication and identification to continuous monitoring and access control. Research efforts can be broadly categorized into three primary domains:

- **Static Authentication**: Systems that authenticate users based on static body positioning (e.g., hand placement) without requiring dynamic movement patterns. This domain emphasizes geometric and radiometric properties captured through static electromagnetic interactions [1], [2].
- **Dynamic Authentication**: Approaches that leverage temporal behavioral patterns such as gait, keystroke dynamics, or gesture-based interactions. These systems exploit both spatial and temporal variations in CSI to capture unique user behaviors [4]–[6].
- **Multi-User Authentication**: Systems designed to simultaneously authenticate or identify multiple users within the same sensing environment, often requiring advanced signal separation techniques [19], [33].

The domain selection fundamentally influences the system design, as static authentication prioritizes spatial resolution and stable feature extraction, while dynamic systems emphasize temporal dynamics and sequence modeling.

2) *Task Definition*: CSI-based biometric systems address three primary tasks:

- **Authentication (Verification)**: Confirming whether a claimed identity matches the biometric signal. This is typically formulated as a binary classification problem (accept/reject) with associated false acceptance (FAR) and false rejection (FRR) rates [10], [38], [76].
- **Identification**: Determining the identity of an unknown user from a set of enrolled candidates. This requires multi-class classification and is evaluated through precision, recall, ROC-AUC, and primarily the EER obtained through a per-class (One-vs-Rest) strategy [16], [33].
- **Continuous Monitoring**: Maintaining user authentication over extended periods, which may involve session management, drift detection, and adaptive thresholding mechanisms [37], [56].

While authentication focuses on one-to-one matching and emphasizes security (low FAR), identification addresses one-to-many scenarios and prioritizes discriminative capacity across the user population. Our work primarily targets closed-set identification for authentication with static palm-based biometrics.

3) *Classification Dimensions*: Our taxonomy classifies CSI-based biometric systems along five fundamental dimensions:

3.1 Sensing Infrastructure: This dimension characterizes the hardware and software toolchain used for CSI extraction. Major categories include the following:

- **Desktop-based platforms**: Intel 5300 NIC [9], [70], [71] and Atheros-based systems [72] require dedicated network interface cards and desktop-class hardware.
- **Embedded platforms**: Raspberry Pi with Nexmon [8], [16], [73] and ESP-based CSI toolkit [77] enable portable, low-cost sensing deployments suitable for IoT scenarios.
- **Commercial Wi-Fi devices**: Some approaches utilize off-the-shelf routers and access points, trading fine-grained CSI access for deployment convenience [60].

3.2 Signal Domain: Systems vary in their operating frequency bands and bandwidth configurations, as follows:

- **Frequency band**: 2.4 GHz vs. 5 GHz operation impacts wavelength-scale interactions and environmental sensitivity. The 5 GHz band offers finer spatial resolution for small-scale biometric features [9], [16], [19].
- **Bandwidth**: 20 MHz, 40 MHz, or 80 MHz configurations determine subcarrier count and spectral diversity, directly affecting feature richness [18]–[20].
- **Signal representation**: Amplitude-only, phase-only, or complex-valued (amplitude + phase) processing strategies determine which physical phenomena are captured [8], [35], [38].

3.3 Feature Engineering: The feature extraction methodology distinguishes systems, as follows:

- **Handcrafted features**: Statistical, spectral, and temporal descriptors derived from domain knowledge (e.g., mean, variance, spectral centroid) provide interpretability but necessitate specialized design, as demonstrated in our work.
- **Deep learning features**: Convolutional Neural Networks (CNN), Recurrent Neural Networks (RNN), and Transformer architectures automatically extract hierarchical representations but sacrifice interpretability [39], [43].
- **Hybrid approaches**: Combining handcrafted and learned features to leverage both physical interpretability and discriminative power [7], [76].

3.4 Learning Model: Classification strategies range from classical machine learning to deep neural networks, as follows:

- **Classical ML**: Support Vector Machines (SVM), Random Forest, K-Nearest Neighbors (KNN), and Gaussian Naïve Bayes offer interpretability and computational efficiency [8], [78], [79].

- **Deep learning**: CNNs for spatial patterns, RNNs/LSTMs for temporal sequences, and Transformers for attention-based modeling capture complex non-linear relationships [80].
- **Ensemble methods**: Combining multiple models to improve robustness and generalization [5], [12], [38].

3.5 Evaluation Protocol: Experimental methodology significantly impacts reported performance, as follows:

- **Data splitting**: Subject-independent vs. session-independent splits prevent different forms of data leakage.
- **Cross-validation**: K-fold strategies with appropriate normalization (applied within folds) ensure unbiased performance estimates.
- **Metrics**: Accuracy, Precision, Recall, F1-score, and ROC-AUC, alongside per-class EER, the Frequency Count of Scores (FCS), and the Gini Coefficient (GC), provide complementary perspectives on system performance.

4) *Positioning of Existing Works*: To facilitate systematic comparison, we present a comprehensive benchmark of state-of-the-art CSI-based biometric authentication systems. Table I compares representative works across the key dimensions of our taxonomy, including hardware platforms, frequency bands, static vs. dynamic approaches, preprocessing methods, and reported performance metrics.

Analysis of Table I reveals several key observations:

- **Hardware Platform Diversity**: While desktop-based Intel 5300 and Atheros platforms dominated early research, recent works increasingly adopt embedded platforms (Raspberry Pi with Nexmon), reflecting a shift toward practical, deployable systems.
- **Frequency Band Selection**: The majority of static authentication systems prefer the 5 GHz band due to its superior spatial resolution for fine-grained biometric features. However, multi-frequency approaches (2.4 + 5 GHz) have emerged for robustness across diverse environments.
- **Static vs. Dynamic Focus**: Most existing works target dynamic authentication (gait, keystroke, gestures), with only a few explicitly focusing on static palm-based biometrics. This gap highlights the novelty of our approach.
- **Preprocessing Gaps**: The systematic use of IQR and MAD filtering for outlier removal is rare in the literature, despite its demonstrated effectiveness in improving model accuracy.
- **Evaluation Metrics**: EER and ROC-AUC reporting is inconsistent across works, making direct performance comparisons challenging. Our work addresses this challenge by providing a comprehensive set of metrics, including per-class EER analyzed in conjunction with both the FCS and the GC.
- **Feature Domain**: Systems utilizing both amplitude and phase information generally outperform amplitude-only approaches, reinforcing the importance of comprehensive signal processing.

Our experimental setup—Raspberry Pi 4B at 5 GHz with Nexmon, static palm-based gathering, IQR/MAD preprocessing, and comprehensive amplitude + phase feature extraction—represents a unique combination within this taxonomy, filling a critical gap in reproducible, embedded static biometric authentication.

B. Identified Gaps

Through systematic analysis of prior work, we identify several critical gaps that limit the practical deployment and scientific reproducibility of CSI-based biometric systems:

- **Lack of Standardization**: The absence of standardized datasets, evaluation protocols, and feature extraction pipelines impedes fair comparison across systems. Different works employ varying preprocessing strategies, feature sets, and validation procedures, making it difficult to assess genuine algorithmic improvements versus methodological differences.
- **Reproducibility Challenges**: Many studies rely on proprietary hardware (Intel 5300, legacy Atheros NICs) or fail to provide

TABLE I: Benchmark Comparison of State-of-the-Art CSI-Based Biometric Authentication/Recognition Systems

Work	Application	Dev. & Tool	Freq.	Model	Passive Mode	Static Acquisition	Features Selection	EER FAR-FRR	ROC-AUC	Amp./Phase	Best Perf. (%)
Lin et al. (2018) [81]	User Auth.	TP-Link TL-WR886N & Intel 5300 CSI & Intel CSI	2.4 GHz	CNN + ResNet	✓	✗	✗	✗	✗	Amp.	98%
Park et al. (2020) [82]	User Auth. LoS/NLoS	Atheros AR9300 & Atheros CSI	5 GHz	Classic	✗	✓	✗	✗	✗	Phase	97.2%
Kong et al. (2021) [19]	Multi-User Auth.	Atheros NIC & Atheros CSI	2.4 & 5 GHz	CNN + RNN	✗	✗	✗	✓	✗	Both	87.6%
Shi et al. (2021) [5]	User Auth.	Intel 5300 NIC & Intel 5300 CSI	2.4 GHz	Deep Learning + Transfer Learning	✗	✗	✓	✗	✗	Both	96.8%
Gu et al. (2021) [9]	User Auth.	Intel 5300 NIC & Linux CSI	2.4 & 5 GHz	Deep Learning	✓	✗	✓	✓	✗	Amp.	94.3%
Gu et al. (2022) [6]	Auth.	Intel 5300 NIC & Intel CSI Tool	2.4 GHz	CNN + SVM	✗	✗	✓	✓	✗	Amp.	92.1%
Wang et al. (2022) [32]	Gait & Respiration Recognition	Intel 5300 NIC & Intel 5300 CSI	2.4 GHz	Deep Learning	✗	✗	✓	✓	✗	Amp.	98.75%
Turetta et al. (2022) [73]	Identity Recognition	RPi 4B & Nexmon	2.4 GHz	CNN	✓	✗	✗	✗	✗	Amp.	98.2%
Zhang et al. (2022) [7]	Gesture Recognition	Intel 5300 NIC & Linux CSI	5 GHz	CNN + GRU	✓	✗	✗	✗	✗	Both	92.7%
Geng et al. (2022) [11]	Pose Estimation	TP-Link AC1750 & CSI Tool	2.4 GHz	Deep Learning + RCNN + ResNet	✓	✗	✗	✗	✗	Both	87.2%
Lin et al. (2023) [38]	User Auth.	TP-Link TL-WR886N & Intel 5300 CSI & Intel CSI	2.4 GHz	Deep Learning + Transfer Learning	✗	✗	✗	✗	✓	Both	97.1%
Kong et al. (2023) [33]	User Auth.	Intel 5300 & Atheros CSI	5 GHz	CNN-RNN + GRU	✓	✗	✓	✓	✗	Both	86.2%
Guan et al. (2023) [16]	Human Occupancy Counting	RPi 4B & Nexmon	2.4 & 5 GHz	SVM	✗	✗	✓	✗	✓	Amp.	96.0%
Bisio et al. (2024) [35]	Human Act. Recog.	Intel 5300 NIC & Intel 5300 CSI	5 GHz	Random Forest	✗	✗	✓	✓	✗	Both	99.92%
Li et al. (2024) [83]	Multi-Person Sensing	Intel AX210 NIC Linux (debugfs) + MatLab	2.4–7.1 GHz	DenseNet + SKNet + Transformer attention	✗	✗	✗	✗	✗	Both	98.6%
Trindade et al. (2025) [8]	User Auth. Access Control	TP-Link Archer C60 & RPi 4B & Nexmon	5 GHz	Classic	✓	✓	✗	✗	✗	Both	99.81%
Ramesh et al. (2025) [12]	Image Reconstruction	Intel AX210 Wi-Fi 6 & FeitCSI tool & Cam. Intel Realsense D435	5 GHz	Deep Learning + Diffusion Models	✗	✓	✗	✗	✗	Amp.	92.0%
Our Work	Multi-User Auth.	TP-Link Archer C60 & RPi 4B & Nexmon	5 GHz	Random Forest & MLP	✓	✓	All	✓	✓	Both	99.54%

complete implementation details, limiting reproducibility. The transition to open-source platforms (Nexmon) and comprehensive documentation is essential for advancing the field.

- **Static Authentication Underexplored:** While dynamic authentication (gait, gestures) has received substantial attention, static palm-based authentication remains relatively unexplored despite its potential for robust, repeatable biometric signatures. This gap motivates our focus on static gathering methodologies.
- **Preprocessing Methodological Gaps:** The systematic application of outlier removal techniques (IQR, MAD) is inconsistently reported and rarely evaluated for their impact on performance. Our work demonstrates that proper preprocessing can yield significant accuracy improvements (up to 5%).
- **Limited Evaluation Metrics:** Many works report only accuracy, omitting critical security-oriented metrics such as EER, FAR, and FRR. This limits understanding of system robustness and practical deployability in security-sensitive applications.
- **Cross-Environment Generalization:** Few studies rigorously

evaluate performance across diverse environments, frequencies, and hardware configurations. The development of domain adaptation and transfer learning techniques for CSI biometrics remains an open research direction.

- **Open Dataset Availability:** The scarcity of publicly available CSI biometric datasets hampers independent validation and comparison. Establishing standardized benchmark datasets would accelerate research progress.
- **Feature Engineering vs. Deep Learning Trade-offs:** While deep learning approaches show promise, the trade-offs between interpretable handcrafted features and learned representations remain underexplored. Our work demonstrates that carefully designed handcrafted features can achieve competitive performance with superior interpretability.

This work directly addresses several of these gaps by providing: (i) a complete, reproducible pipeline using commodity hardware and open-source tools; (ii) rigorous preprocessing methodology with quantifiable performance impact; (iii) comprehensive evaluation met-

rics including per-class EER; and (iv) focus on static authentication as a complementary approach to dynamic systems.

IV. METHODOLOGY: A UNIFIED CSI PIPELINE

This section details the unified methodology developed for the acquisition, processing, and classification of multiple subjects (users) via Wi-Fi CSI, where the gathering device operates in a passive manner and targets static biometric authentication. The proposed pipeline, executed after the CSI data collection described in Section II-K, integrates physics-grounded and data-driven principles to ensure methodological rigor.

The pipeline combines robust preprocessing, energy- and phase-based feature extraction, and systematic model validation within a controlled cross-validation framework. This structure guarantees reproducibility, prevents data leakage, and preserves the physical interpretability of CSI metrics throughout all stages of processing. Figure 1 illustrates the end-to-end workflow of the proposed unified pipeline.

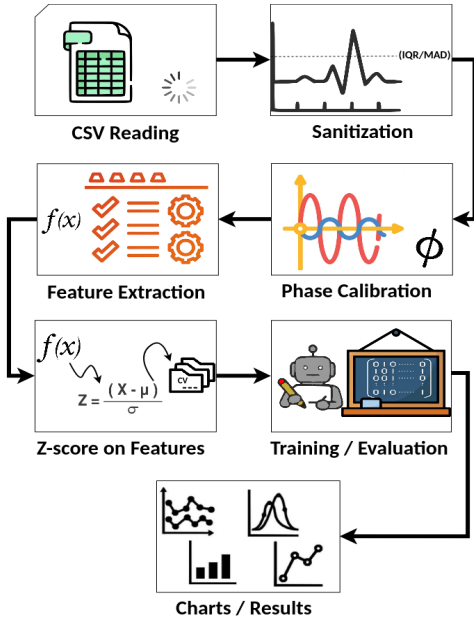


Fig. 1: A Unified Pipeline for CSI-Based Authentication.

A. Preprocessing and Cleaning

Raw CSI readings contain measurement noise and hardware-induced distortions. To ensure statistical consistency and physical plausibility, the pipeline applies a two-stage filtering scheme before feature computation:

- **Subcarrier-level filtering:** Outlier subcarriers are removed using the **Interquartile Range (IQR)** method, discarding frequency bins with energy values outside $[Q1 - 1.5 \times IQR, Q3 + 1.5 \times IQR]$.
- **Sample-level correction:** Temporal anomalies are identified via **Median Absolute Deviation (MAD)** and replaced using linear interpolation over time for both real and imaginary parts.

Phase calibration is then performed using phase unwrapping and detrending to mitigate CFO, SFO, and PDD. This ensures that the residual phase $\phi_{\text{calibrated}}$ represents true propagation effects.

Normalization is applied **only at the feature level**, using Z-score normalization within each fold of cross-validation to prevent data leakage, as discussed in Section IV-C.

It is demonstrably clear that filtering using IQR and MAD is essential for mitigating extreme values caused by hardware noise

and analog front-end impairments. As observed in Figure 2, without this filtering, the unfiltered spectrum (represented by the lighter segments) exhibits amplitudes reaching values exceeding 10 (z-score), consequently leading to a complete distortion of the spectral profile. Post-filtering, the values are constrained to the approximate range of $[-1, 3]$, retaining only the legitimate channel variations induced by the hand’s interaction with the electromagnetic (EM) field. This refinement renders the CSI physically interpretable and suitable for the extraction of reliable and highly discriminative features.

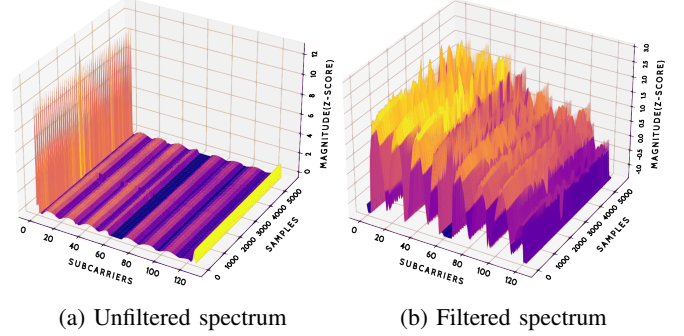


Fig. 2: Spectral Comparison: Unfiltered and Filtered CSI Data from a Single Subject (5-Second Acquisition).

B. Feature Extraction

Feature extraction is grounded in physical and statistical interpretations of CSI. From each cleaned complex matrix $H(f_k, t)$, we derive a structured set of amplitude-, phase-, and spectral-based descriptors, as follows:

- **Amplitude-based features:** Mean, variance, skewness, and kurtosis of $|H(f_k)|$; mean subcarrier energy $E(f_k) = \frac{1}{T} \sum_{t=1}^T |H(f_k, t)|^2$.
- **Phase-based features:** Mean phase $\mathbb{E}[\phi(f_k)]$, standard deviation σ_ϕ , and phase-difference texture $\Delta\phi(f_k) = \phi(f_{k+1}) - \phi(f_k)$.
- **Spectral features:** Spectral centroid, spectral flatness, and spectral entropy from the 1D FFT of averaged magnitude response $\bar{H}(f_k)$.
- **Energy dispersion features:** Ratios of reflected, absorbed, and refracted components computed empirically via $\{|H|^2, \angle H\}$ statistics to represent power redistribution.

This diverse feature space captures both large-scale (energy-level) and fine-grained (spectral-shape) variations in CSI, which are sensitive to the micro-geometry of the human body within the propagation field.

C. Model Training and Validation

To ensure reliability, training was designed under strict isolation principles. Two contrasting scenarios were tested to evaluate potential data leakage:

- 1) **Leak-prone (incorrect):** Normalization applied globally before cross-validation.
- 2) **Leak-free (correct):** Normalization applied within each fold using `StandardScaler` integrated into the pipeline.

If the difference in mean accuracy between both pipelines exceeded 0.01 (1 p.p.), a warning was issued to indicate possible leakage. Only the leak-free pipeline was used in final analyses.

Model optimization was conducted using `GridSearchCV` combined with `StratifiedKFold` ($k = 10$), ensuring class-balanced splits across folds. Parallel execution (`n_jobs = -1`) was enabled to accelerate the hyperparameter search process. The evaluated classifiers included: Decision Tree, Support Vector Machine (RBF Kernel),

K-Nearest Neighbors, Gaussian Naive Bayes, Random Forest and Multilayer Perceptron (MLP).

Performance was evaluated using accuracy, macro-precision, macro-recall, macro-F1, ROC-AUC, and per-class EER. Training time was also measured to compare classical and complex models, showing that tree-based and neural approaches provide higher accuracy at the cost of greater computational effort.

The EER is defined as the point where FAR equals FRR on the ROC curve, serving as a unified indicator of system balance. We adopt a strict threshold of 5.00% as the maximum acceptable value, reflecting a practical trade-off between security and usability. Keeping the EER below this value demonstrates that the system maintains discriminative capability while remaining robust to noise and channel variability—an essential requirement for real-world CSI-based biometric authentication.

The GC quantifies the inequality in error distribution across users, measuring how concentrated authentication errors are among a subset of the user population. Specifically, GC computes the concentration of FAR and FRR at the EER threshold for each user, providing a global average. A high GC value indicates that errors are disproportionately concentrated on a few vulnerable users, revealing an exploitable security vulnerability despite excellent aggregate metrics. Conversely, a low GC value indicates uniform error distribution across all users, ensuring that no individual is disproportionately vulnerable—a fundamental requirement for production deployment in multi-user authentication systems.

The final unified pipeline integrates all previous stages in a reproducible, physically interpretable flow:

This structure ensures that statistical learning aligns with the underlying electromagnetic behavior of the CSI, providing a trustworthy bridge between wireless physics and biometric intelligence.

V. RESULTS AND INSIGHTS

The quantitative evaluation compares multiple classifiers trained on the unified CSI dataset. The evaluation emphasizes precision, specificity ($1 - FAR$), recall ($1 - FRR$), and ROC-AUC in conjunction with the EER per subject. Models such as Random Forest and MLP achieved higher robustness across subjects, confirming the discriminative power of CSI-based features.

A. Quantitative Evaluation

Per-user analysis showed accuracies above 95% for most participants, with minimal confusion between classes. Inter-user variability confirmed that CSI patterns carry distinct amplitude and phase signatures, reinforcing the uniqueness of each individual’s propagation profile. These results confirm the feasibility of static Wi-Fi sensing for reliable biometric identification.

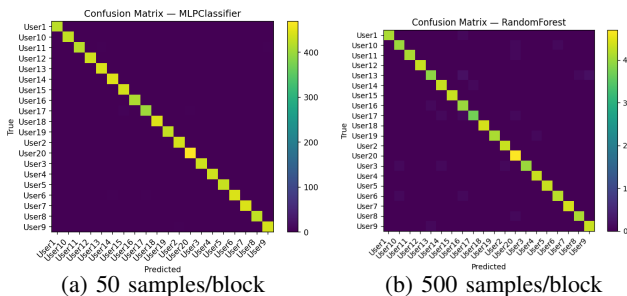


Fig. 3: Comparison among best models - MLP vs. RandomForest

In the confusion matrices, the MLP model (Block Size = 50) exhibits a heavily saturated diagonal, which signifies near-perfect classification accuracy and minimal inter-subject confusion. Conversely, the Random Forest model (BS = 500), while still showing a predominant diagonal, displays off-diagonal values (represented

by green cells) for specific users. This evidence indicates reduced classification precision and greater overlap between the respective classes.

The Random Forest and MLP classifiers, trained with 500- and 50-sample blocks, respectively, achieved the most competitive results across all evaluated metrics (Tables II and III).

TABLE II: Performance Comparison of Classification Models using a 50-Sample Blocks Size

Model	Accuracy	Precision	Recall	F1-score	ROC-AUC	EER-OVR
Decision Tree	94.82%	94.83%	94.83%	94.83%	97.28%	02.71%
SVM (RBF)	98.88%	98.88%	98.88%	98.88%	99.99%	00.24%
KNN	92.54%	92.63%	92.62%	92.50%	99.14%	01.77%
Naive Bayes	69.78%	73.94%	69.76%	69.25%	96.96%	07.31%
Random Forest	99.24%	99.24%	99.24%	99.24%	99.99%	00.24%
MLP	99.54%	99.54%	99.53%	99.53%	99.99%	00.13%

The MLP model demonstrated superior performance among all tested algorithms, consistently yielding EER values below 0.6% and ROC-AUC scores exceeding 99% (Figures 4 and 5). This confirms the MLP’s robustness and high discriminative capability for user-level identification, while also suggesting the underlying relationship between the CSI data and individual subjects is inherently complex.

TABLE III: Performance Comparison of Classification Models using a 500-Sample Blocks Size

Model	Accuracy	Precision	Recall	F1-score	ROC-AUC	EER
Decision Tree	88.72%	88.74%	88.75%	88.68%	94.08%	05.91%
SVM (RBF)	91.39%	91.47%	91.43%	91.39%	99.46%	02.17%
KNN	86.74%	86.74%	86.81%	86.64%	97.02%	03.78%
Naive Bayes	72.09%	75.90%	72.02%	71.60%	96.93%	07.00%
Random Forest	97.44%	97.53%	97.41%	97.43%	99.94%	00.80%
MLP	95.93%	95.94%	95.95%	95.86%	99.86%	00.98%

Both models, despite using disparate block sizes, yielded near-perfect ROC-AUC scores, confirming robust discriminative capacity. The MLP (BS=50) demonstrates that a reduced sample size sufficiently captures unique user signatures. Conversely, the Random Forest (BS=500) shows that while larger blocks enhance stability, they do not surpass the neural network’s capability for fine-grained user separation. Collectively, these findings reinforce the strong presence of biometric information in the CSI data, suggesting that different models explore distinct characteristics (e.g., complexity vs. stability).

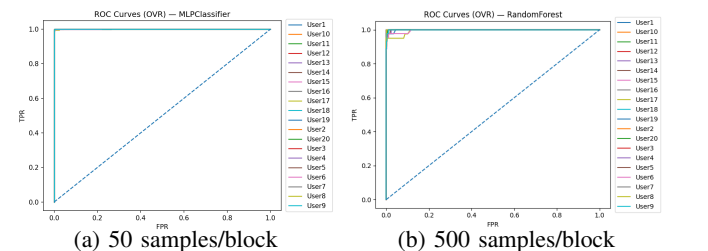


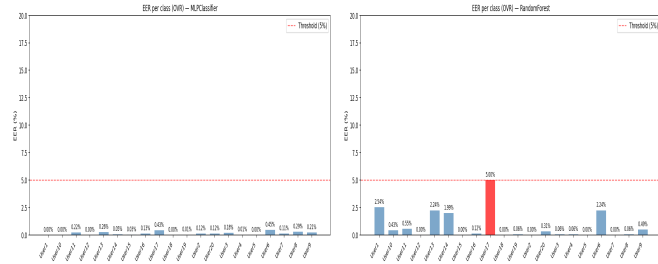
Fig. 4: Comparison among best classifiers - MLP vs. RandomForest

While both models achieve low EER, the MLP trained with 50-sample blocks delivers the most consistent performance, reaching near-zero EER ($< 0.5\%$) across all users. This result is substantially

below the 5% threshold typically considered excellent for biometric systems, reflecting the model’s higher sensitivity to micro-variations in CSI, greater inter-user consistency, and simultaneously lower false acceptance and false rejection rates.

In contrast, the Random Forest using 500-sample blocks maintains reliable performance overall but reaches the 5% EER boundary for one user, indicating slightly reduced robustness. These findings suggest that smaller temporal blocks (50 samples) better preserve fine-grained radiometric features of the hand-channel interaction, enhancing biometric separability—particularly in complex, multi-user CSI scenarios.

The optimal parameters determined for the Random Forest model with a block size of 500 samples are as follows: {classifier_bootstrap: False, classifier_criterion: entropy, classifier_max_depth: None, classifier_max_features: log2, classifier_min_samples_leaf: 1, classifier_min_samples_split: 2, classifier_n_estimators: 200}.



(a) 50 samples/block

(b) 500 samples/block

Fig. 5: Comparison among EER - MLP vs. RandomForest

While for the MLP model with a block size of 50 samples, the optimal parameters determined are presented as: {classifier_activation: tanh, classifier_alpha: 0.1, classifier_hidden_layer_sizes: (50, 50), classifier_learning_rate: constant, classifier_max_iter: 500, classifier_solver: lbfgs}

1) *Model Construction Time*: Additionally, we incorporated a timer to quantify the construction time of the optimal models for both the 500-sample and 50-sample block sizes.

This disparity in computational time stems predominantly from the resulting sample size after feature extraction. The feature dataset constructed with 50-sample blocks will therefore comprise a data volume roughly ten times greater than the dataset generated with 500-sample blocks.

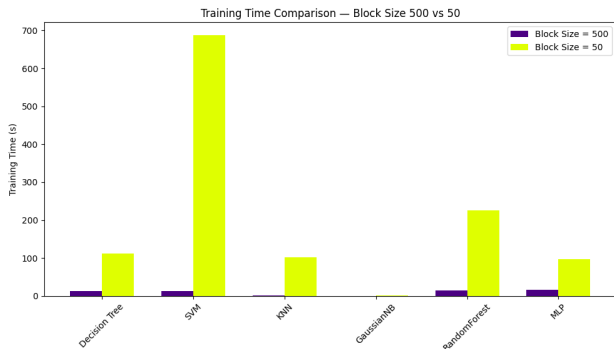


Fig. 6: Impact of Feature Dimensionality on Training Time for ML Classifiers.

B. Feature Importance Analysis

To identify the most discriminative descriptors for CSI-based authentication, we applied the *Minimum Redundancy Maximum Relevance (mRMR)* criterion to 37 extracted features. This method ranks

features by maximizing their mutual information with user identities while minimizing redundancy among them.

The results show that spectral and energy-based descriptors dominate the ranking. In particular, `spectral_centroid_amp`, `energy_reflected_emp`, and `energy_skewness` achieved the highest mRMR scores, indicating strong discriminative power. These features capture how each user’s hand modifies the multipath propagation by absorbing, reflecting, or scattering different subcarrier frequencies (Figure 7).

Lower-ranked features such as `phase_mean_mean` and `dphi_std_mean` showed limited contribution, suggesting that global phase information alone is insufficient without calibration. This confirms that the most relevant biometric traits in static palm-based CSI come from power distribution asymmetry, spectrum morphology, and empirical energy allocation across subcarriers rather than simple amplitude or phase descriptors.

The energetic features yielded crucial insights that may enhance the competitive nature of the system. Energy-based features (Poynting theorem) compute the spectral energy $E(f_k) = |H(f_k)|^2$ and extract statistical descriptors such as skewness, kurtosis, and entropy. They describe how energy is distributed across subcarriers, capturing asymmetry, concentration of spectral peaks, and uniformity, but do not explain the physical mechanism behind these patterns.

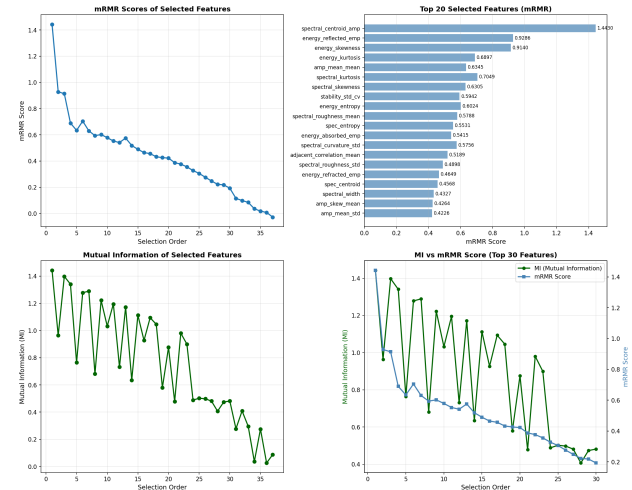


Fig. 7: Selection and Ranking of the Top 15 Discriminative Features using Mutual Information and mRMR Score.

Empirical energy features are derived from the same $E(f_k)$ but decompose it into physical interactions between the hand and the electromagnetic field: *reflected* (energy above the mean), *absorbed* (energy below the mean), and *refracted* (phase dispersion). These quantify how much energy is redirected, lost in tissue, or phase-shifted due to geometry and dielectric properties.

Both groups are complementary: energy-based features answer “*how is energy distributed?*”, while empirical features answer “*what happens to the energy?*”. Together, they provide a physically interpretable and discriminative representation of hand-induced CSI variations, combining statistical uniqueness with biomechanical meaning.

C. Dimensionality Comparison: 37 vs. 15 Features

To evaluate the trade-off between model complexity and performance, two experiments were conducted: one using all 37 features and another restricted to the top 15 mRMR-selected features.

With 15 features, the training time of most models was significantly reduced. For instance, Decision Tree decreased from 112.43 s to 48.40 s, KNN from 102.63 s to 11.14 s, and SVM from 687.14 s to 283.33 s. Random Forest and GaussianNB also benefited from reduced computation.

TABLE IV: Performance Comparison of Classification Models using reduced dimension - 15 features

Model	Accuracy	Precision	Recall	F1-score	ROC-AUC	EER-OVR
Decision Tree	94.56%	94.58%	94.56%	94.56%	97.31%	02.95%
SVM (RBF)	98.91%	98.91%	98.92%	98.92%	99.98%	00.29%
KNN	96.61%	96.62%	96.64%	96.66%	99.32%	00.91%
Naive Bayes	65.80%	69.27%	65.76%	64.50%	96.39%	07.87%
Random Forest	98.73%	98.73%	98.74%	98.73%	99.99%	00.36%
MLP	99.27%	99.27%	99.27%	99.27%	99.98%	00.17%

Importantly, accuracy and EER (as shown in Table IV) remained nearly unchanged for Random Forest and SVM, while a mild degradation was observed in MLP due to its sensitivity to high-dimensional feature interactions. This shows that 15 features preserve most of the discriminative capacity while reducing overfitting risks and computational burden.

Thus, the reduced feature set provides a better balance between interpretability, efficiency, and biometric reliability. However, the MLP model using the full feature space still achieved superior performance, indicating that the additional features—although individually subtle—contribute to improved generalization in real-world situations. In authentication systems, such fine-grained variations may become significant in daily conditions, where environmental and user-induced fluctuations are more pronounced.



Fig. 8: Impact of Feature Dimensionality on Training Time for ML Classifiers.

For the MLP model with a block size of 50 samples using only 15 features, the optimal parameters are as follows: {classifier_activation: tanh, classifier_alpha: 0.1, classifier_hidden_layer_sizes: (50, 50), classifier_learning_rate: constant, classifier_max_iter: 500, classifier_solver: lbfgs}.

VI. DISCUSSION

A. Strengths and Limitations

This study offers several key advantages compared to prior work (Table I):

Accessibility and Reproducibility: Our system leverages low-cost commodity hardware (Raspberry Pi 4B and TP-Link Archer C60) and open-source tools (Nexmon), eliminating proprietary hardware dependencies (e.g., Intel 5300 NIC). This significantly reduces deployment costs and increases accessibility.

Static and Passive Acquisition: The framework operates in passive mode and focuses on static palm-based acquisition, distinguishing it from the majority of literature that relies on dynamic authentication (gait, gestures). The static approach provides repeatable measurements by minimizing motion artifacts.

Systematic Feature Processing: The pipeline integrates a comprehensive preprocessing methodology (IQR and MAD filtering) with

systematic feature selection using the mRMR criterion (Section V-B). This approach optimizes dimensionality and generates quantifiable performance improvements (Section V-C).

Holistic Multi-Metric Evaluation: The evaluation employs comprehensive security-oriented metrics (per-class EER, ROC-AUC, FCS, and GC), providing a holistic assessment of system robustness. This multi-metric approach (Tables II, III, VI, and Section VI-B) reveals critical insights into per-user consistency and vulnerability distribution, which are essential for production deployment.

Dual-Domain Exploitation: The system utilizes both amplitude and phase information from CSI, exploiting the full complex-valued channel response. This dual-domain approach, combined with rigorous phase calibration (Section II-C), captures richer biometric signatures that outperform prevalent amplitude-only systems.

Uniform Security: The Random Forest model demonstrates uniform security across all users (Table VI), ensuring no subject is disproportionately vulnerable to false acceptance or rejection—a fundamental requirement for multi-user authentication in sensitive applications.

Despite its strengths, the current framework exhibits a few notable limitations that must be addressed:

Absence of Anomaly and Drift Mechanisms: The system currently lacks anomaly detection and data drift compensation to distinguish between legitimate user variations and environmental interference or adversarial perturbations. Future work (Section VII-A) must address identifying abnormal patterns (e.g., secondary individuals in the sensing field) which otherwise restrict long-term deployment reliability.

Unvalidated Generalization: The evaluation was conducted exclusively in controlled environments, and cross-environment generalization remains unvalidated. Rigorously evaluating performance across diverse settings, frequencies, and hardware configurations (Section III-B) and developing domain adaptation techniques remain open research challenges.

Trade-offs Despite High Performance: Although the system achieves high aggregate accuracy (99.54% for MLP, 99.24% for Random Forest) and low EER values (0.5%), the MLP model exhibits suboptimal trade-offs (Table V). This indicates that some users may still face undesirable balances between false acceptance and false rejection rates, despite the excellent overall metrics.

B. Complementary Metrics for EER Evaluation

MLP vs. RandomForest under FCS and GC

The MLPClassifier shows top aggregate metrics (very low EER and near-perfect ROC-AUC). However, FCS exposes high between-class variability, with extreme thresholds (≈ 0.03 to ≈ 0.87) and local overlaps between genuine and impostor score distributions. In those classes, the system faces a poor trade-off: either higher FAR or higher FRR. The GC computes the False Acceptance Rate (FAR) and False Rejection Rate (FRR) at the EER threshold for each user and provides a global average [84], as validated in Table V: high GC (notably in FAR) indicates errors concentrated on a few users, i.e., an exploitable vulnerability, despite the excellent average EER.

TABLE V: MLP vs. RandomForest under GC metric

Model	Precision	Recall	GC _{FAR}	GC _{FRR}	GC _{mean}
DecisionTree	94.83%	94.83%	36.51%	36.05%	36.29%
SVM_RBF	98.88%	98.88%	52.86%	44.54%	48.70%
KNN	92.63%	92.62%	51.04%	52.67%	51.86%
GaussianNB	73.94%	69.76%	45.91%	45.16%	45.54%
RandomForest	99.24%	99.24%	45.41%	49.83%	47.62%
MLPClassifier	99.54%	99.53%	66.07%	52.82%	59.45%

Conversely, Random Forest yields slightly worse EER, but a more stable FCS (thresholds mostly mid-range with less overlap) and

moderate GC, meaning more uniformly distributed errors. Practically, Random Forest provides a more predictable trade-off and fewer "vulnerable users" (Figure 9). Implementing the GC within authentication systems enables the identification of potentially "vulnerable users," thereby mitigating breaches and augmenting system robustness.

Takeaway: MLP optimizes average separability (AUC/EER) yet does not ensure risk uniformity (high GC). Random Forest trades a small amount of EER for distributional robustness (lower GC; consistent FCS). For authentication, prioritizing low GC and stable FCS favors Random Forest when per-user reliability matters most.

The MLP model exhibits, in Table VI, a low mean EER (0.13%) but compromises usability and security for a significant portion of the user base due to problematic operational thresholds (70%):

- 40% of subjects are vulnerable to impostors (i.e., operating at an unacceptably high False Acceptance Rate [FAR]).
- 30% of subjects face frequent denial of service (i.e., operating at an unacceptably high False Rejection Rate [FRR]).

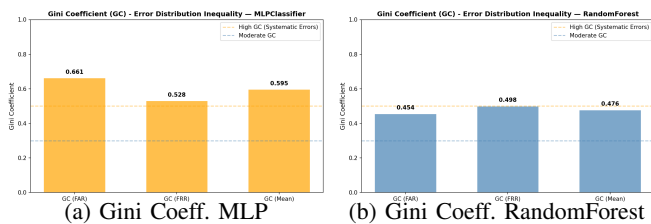


Fig. 9: Comparison of GC between top 2 classifiers - 50 samples/block

In contrast, the Random Forest model, while having a slightly higher mean EER (0.25%), ensures:

- 100% of subjects operate at optimal, balanced thresholds.
- Uniform security across the entire population.
- Uniform usability across the entire population.
- A system ready for production deployment.

1) *Direct Comparison:* An authentication system must function for **all** users, not only for the majority. Random Forest ensures that all users receive comparable protection and exhibit predictable behavior. For biometric authentication, **consistency (RF)** is more important than marginal accuracy gains (**MLP**).

TABLE VI: Direct Comparison between MLP and Random Forest Models

Aspect	MLP	Random Forest	Winner
Variability	0.3693 (σ)	0.1244 (σ)	✓ RF (3× lower)
Extreme Thresholds	14/20 (70%)	0/20 (0%)	✓ RF
Ideal Thresholds	6/20 (30%)	20/20 (100%)	✓ RF
Consistency	✗ Low	✓ High	✓ RF
Uniform Security	✗ No	✓ Yes	✓ RF
Production Readiness	✗ No	✓ Yes	✓ RF

C. Security and Privacy Implications

CSI-based biometric authentication systems, when deployed in scenarios such as credit card transactions, point-of-sale terminals, physical access control, and future online banking applications over Wi-Fi networks, face several security and privacy challenges that must be carefully addressed.

Unlike traditional biometrics (fingerprints, facial recognition [14]), CSI-based signatures are inherently difficult to spoof, as they capture the unique electromagnetic interaction between the user's body geometry and the wireless propagation field. However, potential attack vectors include replay attacks, where an adversary captures and

replays CSI measurements, or sophisticated adversaries attempting to mimic hand geometry and positioning. Our multi-user authentication framework mitigates these risks through the use of Random Forest models, which demonstrate superior consistency and uniform security across all users, a fundamental security requirement for production deployment in sensitive financial and access control applications. (Table VI). Beyond resisting replay-based spoofing, the framework also minimizes the feasibility of geometric imitation attacks, since CSI-based signatures inherently encode not only the external hand geometry but also the complex dielectric interactions of tissues, bones, and blood with the electromagnetic field. This multi-layered physical dependence reduces the likelihood of successful replication and targeted exploitation of vulnerable subjects.

CSI data contains sensitive information about user presence, location, and potentially physiological characteristics. The passive nature of our acquisition methodology (Section II-K) ensures that users need not actively transmit credentials, but the raw CSI measurements themselves could be used for tracking or profiling. To address privacy concerns, feature extraction should be performed locally on the sensing device, with only anonymized feature vectors transmitted to authentication servers. Additionally, the static palm-based approach minimizes the risk of inferring behavioral patterns compared to dynamic authentication systems.

The deployment of CSI-based biometrics in financial and access control contexts requires transparent consent mechanisms, as users may be unaware that their electromagnetic signatures are being captured. The system's high accuracy (99.54% for MLP, 99.24% for Random Forest) and low EER values (<0.5%) provide strong authentication guarantees, but also raise concerns about potential misuse if the technology is deployed without proper safeguards. The reproducible pipeline presented in this work enables independent security audits and validation, contributing to responsible deployment practices.

Our focus on enhancing CSI processing techniques for robust multi-user authentication addresses the critical requirement that authentication systems must function reliably for all enrolled users, not just the majority.

VII. FUTURE DIRECTIONS

To investigate the feasibility of substituting the EER metric with the BioQuake metric [85], [86], we note that the latter inherently computes the EER, the standard deviation (Uncertainty), and the width of the confidence interval (CI Width). Table VII presents results similar to those obtained using the EER metric. The decision to employ either EER or BioQuake is an important consideration, contingent upon available computational resources, as calculating BioQuake requires approximately two to three times the computational effort of the EER metric.

TABLE VII: EER, Std (Uncertainty), and CI Width per Model

Model	EER	Std (Uncertainty)	CI Width
MLPClassifier	0.1309%	0.1010%	0.3795%
RandomForest	0.2465%	0.1088%	0.4469%
SVM_RBF	0.2431%	0.1258%	0.4579%
KNN	1.7708%	0.2897%	1.1443%
DecisionTree	2.7190%	0.4983%	1.9837%
GaussianNB	7.3180%	0.5210%	1.9901%

A. Anomaly Detection and Drift Compensation

Future research directions will address anomaly detection and drift compensation, which are critical for maintaining the reliability and security of CSI-based biometric authentication systems in real-world deployments. **Anomaly detection** focuses on identifying and classifying abnormal patterns in CSI data that deviate from expected user signatures. These anomalies may arise from environmental

interference, such as electromagnetic noise from nearby devices, or from the presence of additional individuals within the sensing field (near-field vs. far-field) [58], [87], which introduces unexpected multipath components and distorts the characteristic CSI signature of the authenticated user. Machine learning-based anomaly detection methods can learn to distinguish between legitimate user variations and genuine environmental or adversarial perturbations, enabling robust operation in complex scenarios.

Data drift represents a fundamental challenge in production CSI-based authentication systems, where the statistical properties of the CSI measurements gradually shift over time due to environmental changes, user physiological variations, or hardware aging [88]. Rather than treating authentication failures caused by drift as simple rejections, these events can be strategically leveraged as security alerts. For instance, in online banking transactions over Wi-Fi networks, when the system fails to authenticate a user due to data drift or anomalous patterns, this failure can trigger a fraud alert mechanism. The financial institution can then associate the transaction with a potential security risk and proactively notify the user through SMS or email, requesting additional authentication verification for the suspicious transaction. This approach transforms authentication failures into an active security monitoring mechanism, enhancing the overall security posture of CSI-based biometric systems while maintaining usability through transparent user communication.

B. IEEE 802.11bf Standardization

The standardization of IEEE 802.11bf makes CSI natively accessible via open MAC signaling, mitigating proprietary firmware dependencies. This change facilitates interoperability and renders the CSI data machine-readable across vendors.

1) *Compatibility and Implementation*: Backward compatibility with 802.11ax/be is maintained through coexistence frames and optional elements. Devices may run in passive (using ambient traffic) or active (dedicated probe) modes. Details such as calibration procedures, temporal stability metrics, and export formats, while also addressing energy, security, and privacy control interfaces, are detailed in [89]—essential for biometric authentication via Wi-Fi.

2) *Research and Application Impact*: Standardized CSI access facilitates multiple research domains:

- **RF-based biometric authentication**, improving repeatability across platforms (e.g., palm-based identification);
- **Vital-sign and activity monitoring**, benefiting from consistent phase fidelity;
- **Occupancy and intrusion detection**, enabled by real-time CSI variation reports.

Furthermore, the unified **sensing** API facilitates embedding ML/AI models at the firmware level, reducing the gap between experimentation and deployment.

3) *Future Directions with 802.11bf*: The standard highlights the following open challenges related to this work:

- **Ensuring the privacy and anonymization of CSI data.**
- **Developing efficient mechanisms for CSI compression and streaming.**
- **Extending sensing capabilities to the 6 GHz and 60 GHz frequency bands to achieve finer spatial resolution.**
- **Integrating federated learning and distributed inference across multiple access points.**

VIII. CONCLUSION

This Systematization of Knowledge examined Wi-Fi CSI biometrics from a security perspective and identified structural inconsistencies that shape the field's evaluation practices. Our taxonomy organizes the space of sensing infrastructures, signal representations, feature pipelines, learning models, and evaluation protocols, clarifying how methodological variability affects robustness and exposure to attacks. Using a unified framework, we showed that common

reporting practices mask security-relevant effects such as uneven per-user risk and inconsistent behavior under realistic perturbations. Metrics such as per-class EER, FCS, and the Gini Coefficient reveal concentrated vulnerabilities that remain hidden under conventional analyses.

These findings indicate that CSI-based biometrics cannot be meaningfully assessed without explicit adversarial models, reproducible pipelines, and evaluation protocols that account for operational threats, including replay attacks, geometric mimicry, and controlled environmental manipulation. The SoK highlights open challenges: cross-environment generalization, temporal drift, limited dataset diversity, and the absence of standardized benchmarks. By consolidating methodological patterns and exposing their security implications, this work provides a foundation for more rigorous and comparable studies of CSI biometrics. It delineates the boundaries within which they can be responsibly considered as authentication primitives, potentially enabling novel proof-of-presence mechanisms for transactions that require physical attestation.

ACKNOWLEDGMENTS

Removed for double-blind review.

REFERENCES

- [1] H. Liu, Y. Wang, J. Liu, J. Yang, and Y. Chen, "Practical user authentication leveraging channel state information (csi)," in *Proceedings of the 9th ACM Symposium on Information, Computer and Communications Security*, ser. ASIA CCS '14. New York, NY, USA: Association for Computing Machinery, 2014, p. 389–400. [Online]. Available: <https://doi.org/10.1145/2590296.2590321>
- [2] S. W. Shah and S. S. Kanhere, "Wi-auth: Wifi based second factor user authentication," in *Proceedings of the 14th EAI International Conference on Mobile and Ubiquitous Systems: Computing, Networking and Services*, ser. MobiQuitous 2017. New York, NY, USA: Association for Computing Machinery, 2017, p. 393–402. [Online]. Available: <https://doi.org/10.1145/3144457.3144468>
- [3] Y. Ma, G. Zhou, and S. Wang, "Wifi sensing with channel state information: A survey," *ACM Comput. Surv.*, vol. 52, no. 3, Jun. 2019. [Online]. Available: <https://doi.org/10.1145/3310194>
- [4] C. Shi, J. Liu, H. Liu, and Y. Chen, "Smart user authentication through actuation of daily activities leveraging wifi-enabled iot," in *Proceedings of the 18th ACM International Symposium on Mobile Ad Hoc Networking and Computing*, ser. Mobihoc '17. New York, NY, USA: Association for Computing Machinery, 2017. [Online]. Available: <https://doi.org/10.1145/3084041.3084061>
- [5] —, "Wifi-enabled user authentication through deep learning in daily activities," *ACM Trans. Internet Things*, vol. 2, no. 2, May 2021. [Online]. Available: <https://doi.org/10.1145/3448738>
- [6] Y. Gu, Y. Wang, M. Wang, Z. Pan, Z. Hu, Z. Liu, F. Shi, and M. Dong, "Secure user authentication leveraging keystroke dynamics via wi-fi sensing," *IEEE Transactions on Industrial Informatics*, vol. 18, no. 4, pp. 2784–2795, 2022.
- [7] Y. Zhang, Y. Zheng, K. Qian, G. Zhang, Y. Liu, C. Wu, and Z. Yang, "Widar3.0: Zero-effort cross-domain gesture recognition with wi-fi," *IEEE Transactions on Pattern Analysis and Machine Intelligence*, vol. 44, no. 11, pp. 8671–8688, 2022.
- [8] E. F. G. Trindade, F. S. de Almeida, G. de Oliveira Braga, R. P. de Mattos Paixão, P. H. dos Santos Rocha, and L. A. P. Jr, "Handpass: A wi-fi csi palm authentication approach for access control," 2025. [Online]. Available: <https://arxiv.org/abs/2510.22133>
- [9] Y. Gu, H. Yan, M. Dong, M. Wang, X. Zhang, Z. Liu, and F. Ren, "Wione: One-shot learning for environment-robust device-free user authentication via commodity wi-fi in man-machine system," *IEEE Transactions on Computational Social Systems*, vol. 8, no. 3, pp. 630–642, 2021.
- [10] S. Han, H. Lee, J. Choi, and E. Hwang, "Multi-frequency band physical-layer authentication in indoor environment," in *GLOBECOM 2023 - 2023 IEEE Global Communications Conference*, 2023, pp. 1741–1746.
- [11] J. Geng, D. Huang, and F. D. la Torre, "Densepose from wifi," 2022. [Online]. Available: <https://arxiv.org/abs/2301.00250>

- [12] E. Ramesh and T. Nishio, "High-resolution efficient image generation from wifi csi using a pretrained latent diffusion model," 2025. [Online]. Available: <https://arxiv.org/abs/2506.10605>
- [13] M. Srinivasan, S. Skaperas, M. S. Herfeh, and A. Chorti, "Joint localization-based node authentication and secret key generation," in *ICC 2022 - IEEE International Conference on Communications*, 2022, pp. 32–37.
- [14] S. S. Vieira. (2025, July) Biometrics are not enough: How advanced fraud is challenging banks. Available online: tiinside.com.br (accessed 2025-11-03).
- [15] M. Schulz, D. Wegemer, and M. Hollick. (2017) Nexmon: The c-based firmware patching framework. [Online]. Available: <https://nexmon.org>
- [16] H. Guan, A. Sharma, D. Mishra, and A. Seneviratne, "Experimental accuracy comparison for 2.4ghz and 5ghz wifi sensing systems," in *ICC 2023 - IEEE International Conference on Communications*, 2023, pp. 4755–4760.
- [17] A. Zhuravchak, O. Kapshii, and E. Pournaras, "Human activity recognition based on wi-fi csi data -a deep neural network approach," *Procedia Computer Science*, vol. 198, pp. 59–66, 2022, 12th International Conference on Emerging Ubiquitous Systems and Pervasive Networks / 11th International Conference on Current and Future Trends of Information and Communication Technologies in Healthcare. [Online]. Available: <https://www.sciencedirect.com/science/article/pii/S1877050921024509>
- [18] Z. Tian, J. Wang, X. Yang, and M. Zhou, "Wicatch: A wi-fi based hand gesture recognition system," *IEEE Access*, vol. 6, pp. 16911–16923, 2018.
- [19] H. Kong, L. Lu, J. Yu, Y. Chen, X. Xu, F. Tang, and Y.-C. Chen, "Multiauth: Enable multi-user authentication with single commodity wifi device," in *Proceedings of the Twenty-Second International Symposium on Theory, Algorithmic Foundations, and Protocol Design for Mobile Networks and Mobile Computing*, ser. MobiHoc '21. New York, NY, USA: Association for Computing Machinery, 2021, p. 31–40. [Online]. Available: <https://doi.org/10.1145/3466772.3467032>
- [20] F. Meneghello, K. F. Haque, and F. Restuccia, "Radio fingerprinting of wi-fi devices through mimo compressed channel feedback," in *IEEE INFOCOM 2025 - IEEE Conference on Computer Communications Workshops (INFOCOM WKSHPS)*, 2025, pp. 1–6.
- [21] Z. Tang, A. Zhu, Z. Wang, K. Jiang, Y. Li, and F. Hu, "Human behavior recognition based on wifi channel state information," in *2020 Chinese Automation Congress (CAC)*, 2020, pp. 1157–1162.
- [22] S. M. Hernandez and E. Bulut, "Wifi sensing on the edge: Signal processing techniques and challenges for real-world systems," *IEEE Communications Surveys & Tutorials*, vol. 25, no. 1, pp. 46–76, 2023.
- [23] —, "Wifi sensing on the edge: Signal processing techniques and challenges for real-world systems," *IEEE Communications Surveys & Tutorials*, vol. 25, no. 1, pp. 46–76, 2023.
- [24] O. O. Oyerinde, "An overview of channel estimation schemes based on regularized adaptive algorithms for ofdm-idma systems," *Digital Signal Processing*, vol. 75, pp. 168–183, 2018. [Online]. Available: <https://www.sciencedirect.com/science/article/pii/S1051200418300216>
- [25] Q. Song, S. Guo, X. Liu, and Y. Yang, "Csi amplitude fingerprinting-based nb-iiot indoor localization," *IEEE Internet of Things Journal*, vol. 5, no. 3, pp. 1494–1504, 2018.
- [26] T. University, "Hands-on wireless sensing with wi-fi: A tutorial," 2023, tsinghua University Wireless Sensing Tutorial. [Online]. Available: <https://tms.thss.tsinghua.edu.cn/wst/docs/pre/>
- [27] D. Avola, M. Cascio, L. Cinque, A. Fagioli, and C. Petrioli, "Person re-identification through wi-fi extracted radio biometric signatures," *IEEE Transactions on Information Forensics and Security*, vol. 17, pp. 1145–1158, 2022.
- [28] Z. Zhou, C. Liu, X. Yu, C. Yang, P. Duan, and Y. Cao, "Deep-wiid: Wifi-based contactless human identification via deep learning," in *2019 IEEE SmartWorld, Ubiquitous Intelligence & Computing, Advanced & Trusted Computing, Scalable Computing & Communications, Cloud & Big Data Computing, Internet of People and Smart City Innovation (SmartWorld/SCALCOM/UIC/ATC/CBDCOM/IOP/SCI)*, 2019, pp. 877–884.
- [29] F. S. de Almeida, E. F. G. Trindade, M. I. Pettersson, R. Machado, and L. A. P. Júnior, "Spider-sense: Wi-fi csi as a sixth sense for early detection in network intrusion detection systems," in *GLOBECOM 2024 - 2024 IEEE Global Communications Conference*, 2024, pp. 2437–2442.
- [30] J. Schäfer, B. R. Barriwal, M. Kokkharova, H. Adil, and J. Liebehenschel, "Human activity recognition using csi information with nexmon," *Applied Sciences*, vol. 11, no. 19, 2021. [Online]. Available: <https://www.mdpi.com/2076-3417/11/19/8860>
- [31] A. Sharma, J. Li, D. Mishra, and A. Seneviratne, "Robust ml model for human counting using ambient wifi traffic from multiple sources," in *2021 IEEE International Conference on Communications Workshops (ICC Workshops)*, 2021, pp. 1–6.
- [32] X. Wang, F. Li, Y. Xie, S. Yang, and Y. Wang, "Gait and respiration-based user identification using wi-fi signal," *IEEE Internet of Things Journal*, vol. 9, no. 5, pp. 3509–3521, 2022.
- [33] H. Kong, L. Lu, J. Yu, Y. Chen, X. Xu, and F. Lyu, "Toward multi-user authentication using wifi signals," *IEEE/ACM Transactions on Networking*, vol. 31, no. 5, pp. 2117–2132, 2023.
- [34] T. Z. Chowdhury, C. Leung, and C. Y. Miao, "Wihacs: Leveraging wifi for human activity classification using ofdm subcarriers' correlation," in *2017 IEEE Global Conference on Signal and Information Processing (GlobalSIP)*, 2017, pp. 338–342.
- [35] I. Bisio, C. Fallani, C. Garibotto, F. Lavagetto, A. Sciarrone, and M. Zerbino, "Analysis of csi-based human activity recognition for contactless patients monitoring," in *GLOBECOM 2024 - 2024 IEEE Global Communications Conference*, 2024, pp. 438–443.
- [36] J. Lv, D. Man, W. Yang, X. Du, and M. Yu, "Robust wlan-based indoor intrusion detection using phy layer information," *IEEE Access*, vol. 6, pp. 30117–30127, 2018.
- [37] X. Cheng and B. Huang, "Csi-based human continuous activity recognition using gmm-hmm," *IEEE Sensors Journal*, vol. 22, no. 19, pp. 18709–18717, 2022.
- [38] C. Lin, P. Wang, C. Ji, M. S. Obaidat, L. Wang, G. Wu, and Q. Zhang, "A contactless authentication system based on wifi csi," *ACM Trans. Sen. Netw.*, vol. 19, no. 2, Mar. 2023. [Online]. Available: <https://doi.org/10.1145/3532095>
- [39] X. Li, H. Yang, C. Yi, R. Deng, and X. Wu, "Anti-noise and cross-domain csi gesture recognition with multi-features fusion transformer," in *GLOBECOM 2024 - 2024 IEEE Global Communications Conference*, 2024, pp. 4191–4195.
- [40] P. Liu, P. Yang, W.-Z. Song, Y. Yan, and X.-Y. Li, "Real-time identification of rogue wifi connections using environment-independent physical features," in *IEEE INFOCOM 2019 - IEEE Conference on Computer Communications*, 2019, pp. 190–198.
- [41] X. Cheng, B. Huang, and J. Zong, "Device-free human activity recognition based on gmm-hmm using channel state information," *IEEE Access*, vol. 9, pp. 76592–76601, 2021.
- [42] Z. Wei, W. Chen, S. Ning, W. Lin, N. Li, B. Lian, X. Sun, and J. Zhao, "A survey on wifi-based human identification: Scenarios, challenges, and current solutions," *ACM Trans. Sen. Netw.*, vol. 21, no. 1, Jan. 2025. [Online]. Available: <https://doi.org/10.1145/3708323>
- [43] G. Diaz, I. Sobron, I. Eizmendi, I. Landa, and M. Velez, "Activity recognition from channel state information for few-sampled scenarios," in *2023 IEEE Globecom Workshops (GC Wkshps)*, 2023, pp. 1009–1014.
- [44] J. Li, D. Mishra, D. Krishnaswamy, A. Chakraborty, J. G. Davis, and A. Seneviratne, "Wifi interference-based adversarial attacks on ntc using csi sensing," in *ICC 2022 - IEEE International Conference on Communications*, 2022, pp. 4354–4359.
- [45] Y. Pu, Y. Jiang, and H.-M. Hu, "Hr-har: A hierarchical relation representation for human activity recognition based on wi-fi," *IET Communications*, vol. 17, no. 1, pp. 29–44, 2023. [Online]. Available: <https://ietresearch.onlinelibrary.wiley.com/doi/abs/10.1049/cmu2.12497>
- [46] H. Dai, W. Shi, Z. Zhou, and J. Jiang, "Authentication method for wifi connection of devices based on channel state information," in *2020 IEEE 6th International Conference on Computer and Communications (ICCC)*, 2020, pp. 37–43.
- [47] L. Xu, X. Zheng, X. Li, Y. Zhang, L. Liu, and H. Ma, "Wicam: Imperceptible adversarial attack on deep learning based wifi sensing," in *2022 19th Annual IEEE International Conference on Sensing, Communication, and Networking (SECON)*, 2022, pp. 10–18.
- [48] M. A. A. Al-qaness, M. Abd Elaziz, S. Kim, A. A. Ewees, A. A. Abbasi, Y. A. Alhaj, and A. Hawbani, "Channel state information from pure communication to sense and track human motion: A survey," *Sensors*, vol. 19, no. 15, 2019. [Online]. Available: <https://www.mdpi.com/1424-8220/19/15/3329>
- [49] Z. Li, F. Ma, A. S. Rathore, Z. Yang, B. Chen, L. Su, and W. Xu, "Wavespy: Remote and through-wall screen attack via mmwave sensing," in *2020 IEEE Symposium on Security and Privacy (SP)*, 2020, pp. 217–232.

- [50] H. Li, C. Xu, A. S. Rathore, Z. Li, H. Zhang, C. Song, K. Wang, L. Su, F. Lin, K. Ren, and W. Xu, "Vocalprint: exploring a resilient and secure voice authentication via mmwave biometric interrogation," in *Proceedings of the 18th Conference on Embedded Networked Sensor Systems*, ser. SenSys '20. New York, NY, USA: Association for Computing Machinery, 2020, p. 312–325. [Online]. Available: <https://doi.org/10.1145/3384419.3430779>
- [51] T. Nakamura, M. Bouazizi, K. Yamamoto, and T. Ohtsuki, "Wi-fi-csi-based fall detection by spectrogram analysis with cnn," in *GLOBECOM 2020 - 2020 IEEE Global Communications Conference*, 2020, pp. 1–6.
- [52] S. Tan, J. Yang, and Y. Chen, "Enabling fine-grained finger gesture recognition on commodity wifi devices," *IEEE Transactions on Mobile Computing*, vol. 21, no. 8, pp. 2789–2802, 2022.
- [53] C. Chen, G. Zhou, and Y. Lin, "Cross-domain wifi sensing with channel state information: A survey," *ACM Comput. Surv.*, vol. 55, no. 11, Feb. 2023. [Online]. Available: <https://doi.org/10.1145/3570325>
- [54] V. V. Ratnam, H. Chen, H.-H. Chang, A. Sehgal, and J. Zhang, "Optimal preprocessing of wifi csi for sensing applications," *IEEE Transactions on Wireless Communications*, vol. 23, no. 9, pp. 10 820–10 833, 2024.
- [55] F. Zhang, C. Wu, B. Wang, H.-Q. Lai, Y. Han, and K. J. R. Liu, "Widetec: Robust motion detection with a statistical electromagnetic model," *Proc. ACM Interact. Mob. Wearable Ubiquitous Technol.*, vol. 3, no. 3, Sep. 2019. [Online]. Available: <https://doi.org/10.1145/3351280>
- [56] C. Wu, F. Zhang, Y. Hu, and K. J. R. Liu, "Gaitway: Monitoring and recognizing gait speed through the walls," *IEEE Transactions on Mobile Computing*, vol. 20, no. 6, pp. 2186–2199, 2021.
- [57] Z. Wu, X. Xiao, C. Lin, S. Gong, and L. Fang, "Widff-id: Device-free fast person identification using commodity wifi," *IEEE Transactions on Cognitive Communications and Networking*, vol. 9, no. 1, pp. 198–210, 2023.
- [58] J. Li, K. Yingchanakiate, D. Mishra, and A. Seneviratne, "Thermal source localization using wifi sensing," in *GLOBECOM 2024 - 2024 IEEE Global Communications Conference*, 2024, pp. 1875–1880.
- [59] O. Oshiga, H. U. Suleiman, S. Thomas, P. Nzerem, L. Farouk, and S. Adeshina, "Human detection for crowd count estimation using csi of wifi signals," in *2019 15th International Conference on Electronics, Computer and Computation (ICECCO)*, 2019, pp. 1–6.
- [60] X. Meng, J. Zhou, X. Liu, X. Tong, W. Qu, and J. Wang, "Secur-fi: A secure wireless sensing system based on commercial wi-fi devices," in *IEEE INFOCOM 2023 - IEEE Conference on Computer Communications*, 2023, pp. 1–10.
- [61] K. Wang, C. Shi, J. Cheng, Y. Wang, M. Xie, and Y. Chen, "Solving the wifi sensing dilemma in reality leveraging conformal prediction," in *Proceedings of the 20th ACM Conference on Embedded Networked Sensor Systems*, ser. SenSys '22. New York, NY, USA: Association for Computing Machinery, 2023, p. 407–420. [Online]. Available: <https://doi.org/10.1145/3560905.3568529>
- [62] J. Ding and Y. Wang, "Wifi csi-based human activity recognition using deep recurrent neural network," *IEEE Access*, vol. 7, pp. 174 257–174 269, 2019.
- [63] F. Meneghello, M. Rossi, and F. Restuccia, "Deepcsi: Rethinking wi-fi radio fingerprinting through mu-mimo csi feedback deep learning," in *2022 IEEE 42nd International Conference on Distributed Computing Systems (ICDCS)*, 2022, pp. 1062–1072.
- [64] X. Lu, J. Lei, Y. Shi, and W. Li, "Physical-layer authentication based on channel phase responses for multi-carriers transmission," *IEEE Transactions on Information Forensics and Security*, vol. 18, pp. 1734–1748, 2023.
- [65] U. Satija, N. Trivedi, G. Biswal, and B. Ramkumar, "Specific emitter identification based on variational mode decomposition and spectral features in single hop and relaying scenarios," *IEEE Transactions on Information Forensics and Security*, vol. 14, no. 3, pp. 581–591, 2019.
- [66] A. Sharma, D. Mishra, S. Jha, and A. Seneviratne, "An investigation into the non-uniformity of channel state information in wifi sensing systems," in *IEEE INFOCOM 2024 - IEEE Conference on Computer Communications Workshops (INFOCOM WKSHPS)*, 2024, pp. 1–6.
- [67] X. Wang, J. Wang, K. Niu, J. Xiong, F. Zhang, E. Yi, A. Yu, Z. Yao, and D. Zhang, "Wi2dmeasure: Wifi-based 2d object size measurement," in *Proceedings of the 22nd ACM Conference on Embedded Networked Sensor Systems*, ser. SenSys '24. New York, NY, USA: Association for Computing Machinery, 2024, p. 253–266. [Online]. Available: <https://doi.org/10.1145/3666025.3699336>
- [68] P. Hu, W. Yang, X. Wang, S. Mao, and E. Shen, "Wiw-m-ep: Wi-fi csi-based wheat moisture detection using equivalent permittivity," in *IEEE INFOCOM 2023 - IEEE Conference on Computer Communications Workshops (INFOCOM WKSHPS)*, 2023, pp. 1–6.
- [69] Z. Yang, Y. Zhang, G. Chi, and G. Zhang, "Hands-on wireless sensing with wi-fi: A tutorial," 2022. [Online]. Available: <https://arxiv.org/abs/2206.09532>
- [70] Y. Gu and X. Yu, "Wipass: Pin-free and device-free user authentication leveraging behavioral features via wifi channel state information," in *2021 3rd International Conference on Advances in Computer Technology, Information Science and Communication (CTISC)*, 2021, pp. 120–124.
- [71] Q. Lu, S. Li, J. Zhang, and R. Jiang, "Pedr: Exploiting phase error drift range to detect full-model rogue access point attacks," *Computers & Security*, vol. 114, p. 102581, 2022. [Online]. Available: <https://www.sciencedirect.com/science/article/pii/S0167404821004041>
- [72] T. Fukushima, T. Murakami, H. Abeysakera, T. Fujihashi, T. Watanabe, and S. Saruwatari, "Feasibility study of practical aoa estimation using compressed csi on commercial wlan devices," *IEEE Access*, vol. 10, pp. 49 128–49 141, 2022.
- [73] C. Turetta, F. Demrozi, P. H. Kindt, A. Masrur, and G. Pravadelli, "Practical identity recognition using wifi's channel state information," in *2022 Design, Automation & Test in Europe Conference & Exhibition (DATE)*, 2022, pp. 76–79.
- [74] F. Gringoli, M. Schulz, J. Link, and M. Hollick, "Free your csi: A channel state information extraction platform for modern wi-fi chipsets," in *Proceedings of the 13th International Workshop on Wireless Network Testbeds, Experimental Evaluation & Characterization*, ser. WiNTECH '19, 2019, p. 21–28. [Online]. Available: <https://doi.org/10.1145/3349623.3355477>
- [75] MSI Global, "Msi gs63 stealth 8re - specification," <https://www.msi.com/Laptop/GS63-Stealth-8RE/Specification>, 2025, accessed: Oct. 24, 2025.
- [76] H. Kong, L. Lu, J. Yu, Y. Zhu, F. Tang, Y.-C. Chen, L. Kong, and F. Lyu, "Push the limit of wifi-based user authentication towards undefined gestures," in *IEEE INFOCOM 2022 - IEEE Conference on Computer Communications*, 2022, pp. 410–419.
- [77] N. Basha, B. Hamdaoui, A. Erbad, and M. Guizani, "On the detection of replay authentication attacks through channel state information analysis," in *GLOBECOM 2024 - 2024 IEEE Global Communications Conference*, 2024, pp. 1719–1724.
- [78] A. Sobehy, E. Renault, and P. Mühlethaler, "Csi-mimo: K-nearest neighbor applied to indoor localization," in *ICC 2020 - 2020 IEEE International Conference on Communications (ICC)*, 2020, pp. 1–6.
- [79] J. M. Rocamora, I.-H. Ho, and M.-W. Mak, "Gaussian models for csi fingerprinting in practical indoor environment identification," in *GLOBECOM 2020 - 2020 IEEE Global Communications Conference*, 2020, pp. 1–6.
- [80] Q. Zheng, B. Liu, and J. Huang, "Compressed representation for 3d human pose estimation using wifi signal," in *2023 4th International Conference on Computer, Big Data and Artificial Intelligence (ICCBDAI)*, 2023, pp. 251–255.
- [81] C. Lin, J. Hu, Y. Sun, F. Ma, L. Wang, and G. Wu, "Wiau: An accurate device-free authentication system with resnet," in *2018 15th Annual IEEE International Conference on Sensing, Communication, and Networking (SECON)*, 2018, pp. 1–9.
- [82] J. Park, H. Kim, and S. Bahk, "Los/nlos detection based authentication for iot systems," in *GLOBECOM 2020 - 2020 IEEE Global Communications Conference*, 2020, pp. 1–6.
- [83] X. Li, H. Wang, Z. Chen, Z. Jiang, and J. Luo, "Uwb-fi: Pushing wi-fi towards ultra-wideband for fine-granularity sensing," in *Proceedings of the 22nd Annual International Conference on Mobile Systems, Applications and Services (MobiSys '24)*. Tokyo, Japan: ACM, 2024, pp. 1–14.
- [84] Y. Hong, L. Qian, M. Zhang, and K. Ren, "A gini coefficient based evaluation metric for continuous authentication systems," *IEEE Transactions on Information Forensics and Security*, vol. 16, pp. 4530–4543, 2021.
- [85] R. Al-Refai, P. P. Ramasamy, R. Ramesh, P. Arias-Cabarcos, and P. Terhörst, "A comprehensive re-evaluation of biometric modality properties in the modern era," 2025. [Online]. Available: <https://arxiv.org/abs/2508.13874>
- [86] M. Fallahi, R. Ramesh, P. P. Ramasamy, P. A. Cabarcos, T. Strufe, and P. Terhörst, "On the reliability of biometric datasets: How much test data ensures reliability?" 2025. [Online]. Available: <https://arxiv.org/abs/2501.06504>

- [87] J. Hu, H. Jiang, T. Zheng, J. Hu, H. Wang, H. Cao, Z. Chen, and J. Luo, "M2-fi: Multi-person respiration monitoring via handheld wifi devices," in *IEEE INFOCOM 2024 - IEEE Conference on Computer Communications*, 2024, pp. 1221–1230.
- [88] K. Kayano, S. Ohta, T. Nishio, D. Yoda, K. Taniguchi, and T. Nabetani, "Experimental evaluation of long-term concept drift and its mitigation in wifi csi sensing," in *2025 IEEE 22nd Consumer Communications & Networking Conference (CCNC)*, 2025, pp. 1–2.
- [89] *IEEE Std 802.11bf™-2025: Amendment 4 – Enhancements for Wireless LAN Sensing*, IEEE Computer Society, LAN/MAN Standards Committee Standard IEEE Std 802.11bf™-2025, September 2025, amendment to IEEE Std 802.11™-2024, as amended by IEEE Std 802.11bh™-2024, IEEE Std 802.11be™-2024, and IEEE Std 802.11bk™-2025. Approved 28 May 2025. Published 26 September 2025. [Online]. Available: https://standards.ieee.org/standard/802_11bf-2025.html